London Road, Bracknell
Berkshire RG12 2SZ

LONDON, METEOROLOGICAL OFFICE
Met.O.11 Technical Note No. 237

The semi-geostrophic weir.

MET O 11 TECHNICAL NOTE No 237

The Semi-geostrophic Weir

by

G J Shutts

July 1986

Abstract

Conventional inviscid theories of flow over smooth orogrpahy assume that boundary streamlines do not separate and that, for steady solutions, the orographic surface is isentropic. Cullen et al (1986) describe an element model based on the Lagrangian form of the semi-geostrophic equations which does exhibit separation even th ough viscous or boundary layer effects are absent.

Further examination of this type of solution is made here with a two-fluid model giving particular emphasis to the implied orographic drag and energy dissipation. Some simple analytic solutions are included which show the onset of separation (usually described as the breakdown of semi-geostrophic theory). It is suggested that a substantial proportion of the measured orographic drag force on mountain ranges such as the Alps may be associated with turbulent energy dissipation immediately downstream of the mountain.

1. Introduction - The 'breakdown' of semi-geostrophy

In recent years it has become evident that the treatment of orography in numerical weather prediction and general circulation models requires improvement. The use of sigma coordinates may have encouraged the view that the dynamical effect of orography can be dealt with in the adiabatic framework of large-scale models. In reality, mountains are not smooth and small-scale orographic features can generate propagating gravity waves, boundary layer separation, turbulent eddies, etc which must, depending on model resolution, be treated as sub-grid scale irreversible physics. It is well-known that the existence of radiating waves, eddy shedding or other transience is required for momentum to be exchanged between solid earth and atmosphere through pressure forces (eg Bannon, 1985). Palmer et al (1986) have suggested that conventional forecast models underestimate the efficiency of this momentum exchange through their failure to represent sub-grid scale gravity wave drag and that this omission is responsible for the appearance of excessively westerly flow, particularly in long integrations. Wallace et al (1983) have achieved a similar effect by introducing an 'envelope orography' which involves using orographic heights greater than that given by the grid-box mean.

At the root of these difficulties is the need to resolve or parametrize the irreversible physical processes which lead to drag. Cullen and Parrett (1986) have shown that even when high-resolution, limited area models resolve the dynamics of flow over steep orography the response is frequently unrealistic. In particular, there is a tendency for the mesoscale response (scale ~ 100 km) to be dominated by gravity wave

propagation at unrealistically large horizontal wavelengths. In a companion paper (Cullen et al, 1986) it is argued that the near-discontinuous structures and separation predicted by semi-geostrophic theory are difficult to realize in finite-difference primitive equation models.

An interesting thought experiment sheds some light on these difficulties. Consider a horizontally stratified, semi-infinite atmosphere at rest and bounded below by a smooth flat surface. This lower surface is now imagined to 'grow' a smooth symmetrical mountain quasi-statically (e.g. a bell-shaped mountain with terrain height h(x) given by $h_m/1+(x/a)^2$ where h_m is the peak height and a is the half-width). Since the surface is initially isentropic, it will remain so as h_m increases until a critical peak height h_c is attained. When h_m exceeds h_c, the potential temperature of a small region on the mountain top will exceed its initial value as the isentropic 'skin' adhering to the mountain punctures allowing potentially warmer interior air to make contact with the boundary. (see Purser and Cullen 1986). Eliassen (1980) has also considered this problem and found an indirect method for calculating the flow field for a particular supercritical case. Some simple analytic solutions help to give a physical picture of the onset of this separation effect for an incompressible atmosphere of uniform potential vorticity. Gill (1981) put forward these solutions as models of the balanced flow created by a homogeneous intrusion in a rotating stratified fluid. Using the absolute momentum $M = fx+v_g$ as a horizontal coordinate it can then be shown that the potential temperature θ satisfies Laplace's equation:

$$\frac{\partial^2\theta}{\partial M^2} + \frac{\partial^2\theta}{\partial Z^2} = 0$$

(NB capital Z is used to denote height when M is the other independent variable)

and solutions may be found using classical potential flow theory (eg Lamb, 1932). Furthermore, Gill showed that the defining equation for the potential vorticity:

$$q = J\left(\frac{M,\theta}{x,z}\right)$$

and the thermal wind solution:

$$f\frac{\partial M}{\partial z} = g\frac{\partial\theta/\theta}{\partial x}_\Theta \quad \text{(using the equations of Hoskins (1975))}$$

can be simplified to the Cauchy-Riemann form:

$$\frac{\partial\theta}{\partial Z} = \frac{\partial x}{\partial M} \text{ and } \frac{\partial\theta}{\partial M} = -\frac{\partial x}{\partial Z}$$

respectively after a suitable non-dimensionalization is made.

A complex potential $F = x + i\theta$ can be defined which is an analytic function of $Y = M+iZ$. By choosing for instance the standard textbook potential for flow past a circular cylinder

$$F(Y) = Y + 1/_Y$$

it is readily shown that:

$$x = M + M/(M^2+Z^2)$$

and

$$\theta = Z - Z/(M^2+Z^2)$$

thereby giving $\theta(x,z)$. (For more details see Gill (1981)). Fig 1a shows this solution in $(x,\frac{Nz}{f})$ space where N is the (constant) Brunt-Vaisala frequency of the undisturbed atmosphere. In this case the mountain ridge has an elliptical cross-section with major axis equal to 2N/f times the peak mountain height (H). The θ contours (Fig 1a) squeeze together at the mountain top and the accompanying geostrophic wind (Fig 1b) has its greatest speed at the foot of the ridge. If the half-width is reduced then the static stability at the mountain top increases until the critical half-width $NH/_f$ is reached (Figs 2a,b). At this point the mountain cross-section appears semi-circular and the static stability is infinite at the mountain top corresponding to the onset of separation. It can also be shown that the mountain surface is a constant M surface implying zero absolute vorticity measured on the terrain surface. The non-dimensional solution corresponding to Fig 2 is:

$$\left.\begin{aligned} \theta &= (r^2-1)^{1/2} \text{ Sin } \eta \\ \text{and} \\ v_g &= (r - (r^2-1)^{1/2}) \text{ Cos } \eta \end{aligned}\right\} \quad r \geq 1$$

where (r, η) are polar coordinates.

Analytic solutions for smaller half-widths where the mountain surface is not isentropic have not been found though inviscid piece-wise constant solutions could in principle be obtained by the geometric method described by Cullen et al (1986).

A finite-difference, primitive equation model simulating the growing mountain problem would have great difficulty at the onset of separation since thermal wind balance of the intense gradients near the mountain would not be easily maintained and would lead to spurious inertia-gravity waves. Numerical diffusion would also be required to control the integration and thereby provide a spurious energy sink.

The solutions of Figs 1 and 2 are unaltered by the addition of a uniform geostrophic wind across the ridge. The total flow then follows the isentropes with a speed proportional to their gradient. Peak wind speeds are attained at the mountain crest as noted by several authors (Merkine, 1975; Pierrehumbert, 1985 and Blumen and Gross, 1986). The infinite mountain top wind speed predicted for the semi-circular ridge case is usually interpreted (Pierrehumbert, 1985) as the breakdown point of semi-geostrophic theory. It appears to occur when the radius of curvature of the mountain surface measured in $(x, Nz/_f)$ space falls below the Rossby radius of deformation based on the height of the mountain. For instance a triangular mountain, no matter how high, always causes separation if 'grown' from a flat isentropic surface. This breakdown of semi-geostrophic theory is, in fact, only the point at which solutions obtained by the geostrophic momentum coordinate transformation become multi-valued. As Cullen (1983) has shown for the zero potential vorticity front, this does

not prevent one from constructing solutions in physical space which are fully consistent with the equations of motion expressed as Lagrangian conservation laws. Even so, for the supercritical mountain problem with uniform geostrophic wind, the semi-geostrophic requirement $\frac{D}{Dt} \ll f$ will in general be invalid over a certain finite volume of fluid. We proceed on the basis that if this volume is small compared to the mountain volume then semi-geostrophic solutions will be physically relevant.

Breakdown of semi-geostrophic theory was also encountered in the two-fluid density current model of Davies (1984). In this analytic study, Davies was able to find an expression for the rate of advance of the forward edge of a geostrophic density current as it encountered a smooth mountain. Infinite propagation speeds were predicted if the current lost stability at some point on the mountain. This paper tackles a rather similar problem using a geometric method for solving the semi-geostrophic equations in their Lagrangian conservation form. Solutions can still be obtained after this 'slipping point' is reached. These imply an instantaneous transfer of fluid from the slipping point to a new equilibrium position downstream. We imagine that this extreme example of geostrophic adjustment can be accomplished in reality by a 'weir' flow and that the necessary energy loss can result from processes which do not substantially violate the basic Lagrangian conservation of absolute momentum, entropy and mass.

2. Model formulation

(a) Cold air dome on a horizontal plane

Consider an atmosphere composed of two isentropic fluids, such that, in a Cartesian coordinate system, variations in the y-direction may be ignored (two-dimensional assumption). If the atmosphere is bounded from below by an infinite horizontal plane then a finite volume of the potentially cooler of the two fluids will form a 'dome' in cross-section (Fig 3). It will be assumed throughout that the depth of the cold dome is always very much less than the finite depth of the isentropic atmosphere (H_θ) based on the potential temperture of the ambient warmer air (typically about 30 km). The depth of the cold air will also be assumed to be much less than the density scale height based on the mean temperature of the cold air so that the flow can be considered incompressible. In the geostrophic and hydrostatically balanced equilibrium state with zero geostrophic wind in the warm 'environment', the dome will be supported by a geostrophic wind field v_g (in the y-direction) in accordance with the Margules formula for the slope of a front. The mean vorticity in the dome will be anticyclonic with all the vertical shear concentrated in a vortex sheet at the dome boundary. If the potential temperature of the environment is θ_o and that of the cold air dome is $\theta_o - \Delta\theta$ ($\Delta\theta>0$) then:

$$\frac{dz}{dx} = - \frac{f[M]}{g\Delta\theta/\theta_o} \qquad (1)$$

where z(x) represents the dome interface profile, f is the Coriolis parameter; g, the acceleration due to gravity and [M] represents the difference in absolute momentum ($M = v_g+fx$) measured across the

interface. Changes of v_g in the environmental flow due to vortex compression over the depth of the atmosphere are small and are given by the following scale argument. If the dome interface is lifted a height h_d over a horizontal scale L_d then the change in vorticity in the atmospheric column above will be ~ fh_d/H_θ implying height-independent) changes to $v_g \sim L_d f h_d/H_\theta$.

Taking h_d ~ 1 km, $f \sim 10^{-4}$ s^{-1}, L_d ~ 300 km and H_θ = 30 km consistent with the model to be described, gives a change in v_g above the dome of 1 ms^{-1}. It can be verified a posteriori that M in the environment fluid is well approximated by fx on the basis of these small variations in v_g. Alternatively, this model is exact if the two fluids are of constant density, incompressible and the environment extends to infinity.

Each element in Fig 3 will be considered to have a uniform absolute momentum value, M_i, (i = 1,N). The interface equation (1) then becomes:

$$\frac{dz}{dx} = \frac{f\theta_o}{g\Delta\theta} (M_i - fx)$$

for each element i, and may be integrated to give:

$$z - z_i = \frac{f\theta_o}{g\Delta\theta} [M_i(x-x_i) - {}^1/_2 f(x^2-x_i^2)] \qquad (2)$$

where (x_i,z_i) denotes the position of the left-hand corner of

element i. The right-hand corner of element i therefore satisfies the equation:

$$z_{i+1} - z_i + \frac{f\theta_\Theta}{g\Delta\theta}\left[\frac{1}{2}f(x_{i+1}^2 - x_i^2) - M_i(x_{i+1}-x_i)\right] = 0 \qquad (3)$$

and so for the complete problem of N elements we may write this as:

$$F_i(\underline{X}) = 0 \qquad i = 1, N \qquad (4)$$

where $\underline{X} = (x_1, z_1, x_2, z_2, x_3 \ldots\ldots x_{N+1}, Z_{N+1})$ and F_i is the function represented in eq. (3).

Area conservtion of the fluid elements may be enforced by requiring that:

$$\int_{x_i}^{x_{i+1}} z(x)dx = A_i \quad i = 1, N$$

where A_i, i = 1,N are the initially defined constant areas. Using Eq. (2) this can be shown to be:

$$z_i(x_{i+1}-x_i) + \frac{f\theta_\Theta}{g\Delta\theta}\{\frac{1}{2}M_i(x_{i+1}-x_i)^2 - \frac{f}{6}(x_{i+1}^3 - 3x_i^2x_{i+1} + 2x_i^3)\} - A_i = 0$$

or by defining a function G_i consistent with this:

$$G_i(\underline{X}) = 0 \qquad i = 1, N \qquad (5)$$

Now (4) and (5) represent a total of 2N equations involving the 2(N+1) components of the vector $\underline{X}$ and, of course, the problem is not correctly posed until two boundary conditions are included. These simply require that (x_1, z_1) and (x_{N+1}, z_{N+1}) lie on the lower boundary if the interface is to represent a dome. If the lower surface is a horizontal plane then:

$$z_1 = 0$$
$$\text{and} \qquad z_{N+1} = 0 \qquad . \qquad (6)$$

are the missing equations needed to define the problem.

Given the values of M_i and A_i at any time then the geometry of the dome is uniquely determined by eqs. (4)-(6). Suppose now the imposition of a uniform geostrophic current U_g in the the x-direction. The y-component of the momentum equation can, under the semi-geostrophic assumption, be written as:

$$\frac{DV}{Dt}g + fu + \frac{\partial \phi}{\partial y} = 0 \qquad (7)$$

where u is the wind speed (including agestrophic component) in the x-direction and ϕ is the geopotential, (see Hoskins and Bretherton (1972)). Furthermore, this may be simplified to:

$$\frac{DM}{Dt} = fU_g \qquad (8)$$

Using the geostrophic wind relation and, because U_g is a constant, eq. (8) can be integrated for each element to give:

$$M_i(t) = M_i(0) + f\, U_g\, t \qquad (9).$$

If the dome sits on a horizontal plane then the effect of this linear increase of M in time is to cause a shape-preserving translation of the interface at the speed of the geostrophic wind. Changes in the dome interface profile will occur if there is 'orography' at the lower boundary.

(b) Flow over a rectangular block mountain

Consider the initial state indicated in Fig 4(a) with a triangular wedge of cold air supported by a rectangular block mountain. The cold air extends half-way up the 2 Km high mountain and 1000 km upstream. The absolute momentum distribution before sub-division into elements is given by:

$$M = fx + \Delta M$$

so that a constant difference ΔM along the interface implies that it is straight. The cold air is then partitioned into 39 elements of equal area A_i and M_i is set equal to $^1/_2\, f(x_i+x_{i+1}) + \Delta M$ using the x_i's obtained from the sub-division. The boundary conditions (eqs. 6) now become:

$$z_1 = 0$$

$$x_{N+1} = 0$$

so that the dome is forced to make contact with the vertical mountain side at x = 0. These conditions together with eqs. (4) and (5) constitute a set of nonlinear algebraic equations for the vertex coordinates (x_i,z_i) given M_i and A_i. Roots were obtained using a NAG library routine (C05PBF) which is based on a modification of the Powell hybrid method (Powell, 1970). A first guess for (x_i, z_i) is required though it was found that this does not have to be very accurate in order to find a solution.

As M_i increases linearly in time in accordance with eq. (9), sets of (x_i,z_i) are obtained, two of which are plotted in Figs 4(b) and (c). The cold air moves at a speed less than the geostrophic wind due to the blocking influence of the mountain and the interface rises until it becomes tangential to the top left-hand corner of the mountain. The tail-end of the cold wedge initially travels at a speed only slightly less than the imposed 5 ms^{-1} geostrophic wind speed consistent with an upstream blocking influence of order $(\frac{g\Delta\theta}{f^2\theta_o} z_{n+1})^{1/2}$ ~ 150 km. (Cullen et al, 1986). Since the element next to the mountain is unable to move to larger x, v_g increases in time leading to a strong (~ 30 ms^{-1}) jet along the mountain ridge axis. When the interface becomes tangential to the mountain surface as in Fig 4(c) the solution cannot make physical sense without losing fluid from the upstream cold air wedge. At this point the area conservation requirement is relaxed in the element against the mountain and replaced with the condition that $z_{N+1} = h_m$ (the mountain height) so that the vertex (x_{N+1},z_{N+1}) coincides with the mountain corner. The solution can then be continued with A_N

decreasing to zero, after which element N is assumed to have crossed the ridge leaving N-1 elements. The process is continued so that one by one the elements disappear from the upstream side of the ridge.

While elements are blocked by the mountain ridge they acquire large absolute momentum values. When they are in the process of 'leaking' over the ridge, fluid jumps discontinuously to a new equilibrium position downstream where M values are roughly the same as the environmental absolute momentum, fx. As for the upstream cold air, a new equilibrium dome may be calculated based on how many elements have crossed the ridge and what fraction of the 'in-transit' element has jumped over. Physically, air released at the mountain crest has a Coriolis force f[M] acting on it which coupled with buoyancy causes a 'weir-like' acceleration towards a new downstream equilibrium position. Figs 4(d) and (e) show successive flow states at later times. Shortly after the first element crosses the ridge the downstream dome makes contact with the 100 Km wide mountain and the boundary conditions have to be modified accordingly. Later the whole dome moves away from the mountain as the subsequent mass transfer rate across the ridge slows down. It moves with a speed close to the geostrophic wind speed in the absence of any obstacle. Clearly, for mountain ridges narrower than the 100 km chosen here the solution is barely different. In fact the lee slope can take on any configuration and give identical solutions (eg infinitely thin razor-blade ridge) provided that it does not intersect the sequence of equilibrium

profiles of the downstream dome. The dominant mountain parameter is the height of the vertical windward face which dictates how long the air will be delayed in its transit.

Perhaps the most important aspect of this geometric solution is the pressure force exerted on the mountain block. The pressure difference $\Delta p(z)$ cross the mountain corresponding to Fig 4(e) is given by:

$$\Delta p = \rho_o \frac{g\Delta\theta h_m}{\theta_o} (1 - \frac{z}{h_m})$$

so that the net pressure force D per unit length along the ridge is:

$$D = \int_o^{h_m} \Delta p \, dz = \rho o \frac{g\Delta\theta h_m}{\theta_o}[z - \frac{z^2}{2h_m}]_o^{h_m} = \rho o \frac{g\Delta\theta}{2\theta_o} h^2_m$$

Using $\rho_o \sim 1$ Kgm^{-3}, $g \sim 10$ m^{2}s^{-1}, $\Delta\theta = 5°K$, $\theta_o = 300°K$ and $h_m \sim 2$ Km gives:

$$D \sim 3.4 \times 10^5 \text{ N m}^{-1}$$

or a total force of 3.4 N m^{-2} acting over the area of the mountain which compares favourably with observed estimates made by Davies and Phillips (1985) using ALPEX data.

Rather than dwell on the results obtained from this extreme mountain problem it is more instructive to consider a standard, smooth mountain model and make a more detailed analysis of the predicted drag and energetics.

(c) The bell-shaped mountain

The principal complication introduced by considering smooth orography such as the bell-shaped mountain (whose height $h(x) = h_m a^2/(a^2+x^2)$) is that , unlike the rectangular block mountain case, the point at which stability is lost is not known a priori and even then it changes with time. Nevertheless, in practice, it turns out to be little harder to use the element model in this case, particularly since the orographic profile is specified by a single equation rather than the five straight lines which represent the rectangular block case. The Margules equations (4) are clearly independent of the shape of the orography and it is the area conservation requirement eq. (5) that must be modified. Since elements are raised as they move towards the mountain peak the area under the fluid interface between x_i and x_{i+1} must include the area under the mountain profile ie.

$$\int_{x_i}^{x_{i+1}} z(x)dx = A_i + \hat{A}\ (x_i, x_{i+1})$$

where $\hat{A}\ (x_i, x_{i+1}) = \int_{x_i}^{x_{i+1}} h(x)dx = ah_m[\mathrm{Tan}^{-1}(x_{i+1}/a) - \mathrm{Tan}^{-1}(x_i/a)]$

for the bell-shaped mountain. Eq. (5) can then simply be adapted by replacing A_i with $A_i + \hat{A}\ (x_i, x_{i+1})$. The cold air is initially assumed to take the form of a shallow, two-dimensional dome upstream of the ridge. The boundary condition equations required in conjunction with eq. (4) and the modified eq. (5) simply express that (x_1, z_1) and (x_{N+1}, z_{N+1}) satisfy the orographic profile equations:

$$z_1(a^2+x_1^2) - h_m a^2 = 0 \qquad (10)$$

and $z_{N+1}(a^2+x^2_{N+1}) - h_m a^2 = 0$

The initial configuration of this dome together with its associated v_g profile are shown in Fig 5(a) for a mountain of height h_m = 2 Km and half-width a = 50 Km - typical of a smoothed cross-section through the Swiss Alps. All other parameters are identical to those chosen for the rectangular mountain case. If the x-axis points eastwards then the peak value of v_g on the upstream side of the dome corresponds to a southerly wind of 8 ms^{-1}. Since the dome is already some way up the mountain a smaller northerly wind occurs at the leading edge. By increasing the M values for all elements linearly in time, a sequence of dome configurations can be obtained during the ascent of the mountain. When the interface slope at the leading edge of the dome becomes equal to the mountain slope then stability is lost and a weir begins. This is indicated when a solution to the algebraic equations cannot be found under the boundary conditions (10). For the physical parameters chosen here this happens just before the cold air reaches the summit. At the onset of the weir the area conservation equation $G_N(\underline{X}) = 0$ is replaced by an equation which expresses the tangency of the interface to the mountain surface ie.

$$\left.\frac{dz}{dx}\right|_{x_{N+1}} = \frac{f\theta_o}{g\Delta\theta}(M_N - fx_{N+1}) = \left.\frac{dh}{dx}\right|_{x_{N+1}}$$

or

$$\frac{f\theta_o}{g\Delta\theta}(M_N - fx_{N+1}) = -2a^2h_m\, x_{N+1}/(a^2+x^2_{N+1})^2 \qquad (11)$$

using Margules' formula. Solution of the new algebraic equation set then allows one to calculate the new area of the N th element and find out how much fluid has been lost to the lee-side of the ridge. This process can be continued for later times until the area is found to be negative, at which point all of element N has escaped and the configuration of the remaining N-1 elements is sought. At the instant that an element completes its passage over the mountain the next element will be below its 'slipping-point' and a short period of time elapses before it too flows over the mountain. This is because the interface slope is discontinuous at element boundaries and so the tangency condition cannot be enforced continuously over the time during which weir elements change. For most of the time integration this short build-up phase was not encountered and the tangency condition eq. (11) could be used at each timestep after the weir had begun. Again, a lee-side dome could be constructed given a reasonable first guess. This was obtained initially (when two elements had crossed the ridge) by constructing the dome on a flat horizontal surface by setting h_m equal to zero and then repeatedly constructing the geometry as the ridge was 'grown' to its correct height profile. After this, first guesses where obtained from the previous timestep coordinates (x_i, z_i).

Figs 5(b)-(f) show the resulting dome configurations at selected times together with v_g profiles. The first cold air to cross the mountain falls more or less to the foot of the lee slope and acquires a northerly wind in contrast to the southerly jet developing on the windward side, Fig 5(b). Note that for the element currently crossing

the summit both portions of it making up the two domes have the same absolute momentum. Since they are located at different positions along the x-axis they are accompanied by different geostrophic velocities, v_g. Therefore conservation of absolute momentum in the implied weir between the upstream and downstream domes causes the southerly wind at the summit to turn into a northerly at the foot of the lee-slope. At later times the lee-side dome simultaneously extends up the mountain and further downstream (Fig 5(c)). Notice that at all times the depth of cold air on the windward side is greater than that on the lee-side giving a pressure force on the mountain. As the supply of cold air crossing the mountain diminishes, so it becomes more difficult to support the cold air in its passage. Steep interface slopes implying large M are required to get the last few elements across the mountain and this in turn produces a strong southerly jet (~ 20 ms^{-1}) along the ridge (Figs 5(d)-(f)). Finally, when all the cold air has crossed the mountain and moved downstream the shape of dome is identical to its original shape on the upstream side since M_i, θ_i and A_i are conserved. During the intervening time the dome obviously has a higher centre of mass and greater kinetic energy so that work must have been done by the basic state pressure field in association with U_g. An analysis of the energy transformations implied by this sequence of equilibrium states will now be shown to be consistent with the drag force on the mountain.

3. Energetics and orographic pressure force

Since the mountain ridge can do no work on the flow, the energy required to raise the centre of mass of the cold air must be provided by the geostrophic flow in the x-direction. In this two-dimensional formulation the basic state geostrophic wind does not change in time and the energy is provided by cross-isobaric flow. To show this consider the equation of motion for the y-direction in Eulerian form:

$$\frac{\partial v_g}{\partial t} + u\frac{\partial v_g}{\partial x} + w\frac{\partial v_g}{\partial z} + fu + \frac{\partial \phi}{\partial y} = 0 \qquad (12)$$

the hydrostatic equation:

$$\frac{\partial \phi}{\partial z} = \frac{g\theta}{\theta_o} \qquad (13)$$

and the incompressibility condition:

$$\frac{\partial u}{\partial x} + \frac{\partial w}{\partial z} = 0 \,. \qquad (14)$$

Multiplying eq. (12) by v_g and eq. (13) by w and then adding can be shown to give:

$$\frac{\partial E_g}{\partial t} + \frac{\partial}{\partial x}\{u(E_g+\phi)\} + \frac{\partial}{\partial z}\{w(E_g+\phi)\} + \frac{\partial}{\partial y}(\phi v_g) = 0 \qquad (15)$$

with $E_g = \frac{1}{2} v_g^2 - \frac{g\theta z}{\theta_o}$ and where eq. (14) and the geostrophic wind relation, $fv_g = \frac{\partial \phi}{\partial x}$, have been used. Integrating eq. (15) over the whole

domain with the assumption that the upper and lower surfaces are rigid (or are unable to support an energy flux) and that $u(E+\phi)|_{x\to\infty} = u(E+\phi)|_{x\to -\infty}$ then gives:

$$\frac{d\overline{E}}{dt}g = -\frac{\partial\overline{\Phi v}}{\partial y}g = fU_g\,\overline{v}_g \qquad (16)$$

where the overbar denotes an integral over the (x, z) plane. Therefore, the existence of a net mass transport in the y-direction (down the basic state pressure field) provides the energy source needed to allow the cold air dome to cross the orographic ridge. Using the geostrophic wind solution for v_g it is easy to show that eq. (16) may be written as:

$$\frac{d\overline{E}}{dt}g = U_g \int_{\infty}^{\infty}(\phi\,\frac{dh}{dx})\,dx = U_g \times \text{drag force}. \qquad (17)$$

Eq. (17) only applies in the absence of unbalanced motion where ageostrophic components to the kinetic energy are negligible. When the weir has been set up, $\overline{E}_g$ must be replaced by $\overline{E} = {}^1/_2(u^2+v^2+w^2)$ in eq. (17). Since the semi-geostrophic model only represents sequences of balanced states with total energy $\overline{E}_g$, then $\overline{E}$ and $\overline{E}_g$ will diverge after the onset of the weir implying an energy sink $\frac{d}{dt}(\overline{E}-\overline{E}_g)$

To help understand the physical significance of this energy sink consider a similar non-rotating problem consisting of a liquid in a two-dimensional tank partitioned by a solid obstacle of height greater than the liquid depth (Fig 6(a)). If the obstacle is moved quasi-statically from right to left the levels of the liquid on either side become unequal and work is required to raise the overall centre of gravity of the liquid

Fig 6(b). The work done against the pressure force on the obstacle is equal to the increase in potential energy of the system until fluid spills over Fig 6 (c). Kinetic energy released as fluid falls will in practice set up surface gravity waves and turbulence which will ultimately be dissipated by viscosity. A balanced model of this system would only 'see' static equilibria with horizontal liquid surfaces on either side of the obstacle. Energy dissipation would be implicit and given by the difference between the rate of working of the obstacle and the rate of change of the potential energy in the system.

In the element model, the excess pressure δP_i at the surface due to the overlying cold air in element i is given by:

$$\delta P_i(x,t) = [z(x,t)]_i - h(x)$$

which, on using the non-dimensional form of eq. (2)

$$z = z_i + M_i(x-x_i) - {}^1/_2\,(x^2-x_i^2)$$

gives:

$$\delta P_i = M_i x - {}^1/_2\, x^2 + z_i - M_i x_i + {}^1/_2\, x_i^2 - h(x) \qquad (18)$$

The excess force F_i exerted on the mountain by element i is then given by:

$$F_i = \int_{x_i}^{x_{i+1}} \delta P_i(x,t)\,\frac{dh}{dx}\,dx = -2h_m \int_{x_i}^{x_{i+1}} \frac{x\,\delta P_i}{(1+x^2)^2}\,dx$$

which using eq. (18) can be expanded into standard integrals. The net force F on the mountain ridge is then simply given by:

$$F = \sum_{i=1}^{N} F_i$$

In order to express this in conventional drag force units, F is divided by 4 mountain half-widths which roughly represents the horizontal extent of the ridge. The time evolution of this drag force is given in Fig 7.

The peak value of ~ 1.3 N m^{-2} occurs soon after the onset of the weir decreasing thereafter as the cold air transfers to the lee-side of the ridge. Note that this value does not depend on the speed of the geostrophic wind crossing the ridge. The area under the curve in Fig. 7 is proportional to the total work extracted from the basic state pressure field and can be equated to the total energy dissipated during the passage of the cold dome over the ridge.

The total semi-geostrophic energy of the system at any time can be evaluated as the sum of kinetic energies, K_i given by:

$$K_i = \int_{x_i}^{x_{i+1}} \frac{1}{2} (M_i - x)^2 \, (z(x) - h(x)) dx$$

and potential energy P_i given by:

$$P_i = \frac{1}{2} \int_{x_i}^{x_{i+1}} \{ [z(x)]_i^2 - h^2(x) \} dx$$

over all elements (i=1, N). Using the analytic form of h(x) it can be shown that K_i+P_i are expressible analytically in terms of M_i, x_{i+1}, x_i and z_i. Fig 8 shows the total work done by the drag force E(t) and the semi-geostrophic energy $E_g = \sum_{i=1}^{N} (K_i+P_i)$, the former being defined to be equal to E_g at t=0.

The two energy curves more or less coincide (as they should do) up until the onset of the weir. Thereafter the model energy E_g levels off and then falls back to its original value as the cold air dome reforms downstream of the ridge. The drag force continues to do work until only the last element remains to cross the ridge.

It is of some interest to relate the total amount of energy dissipated during the dome's transit to a temperature change assuming that the resulting heat energy uniformly warms the cold air. The total heat energy (from Fig 8) is ~ 1.72×10^{11} Joules and can be shown to warm the 5×10^8 Kg of a cold air making up the dome (based on a density of 1 Kg m^{-3}) by 0.034°K using a specific heat at constant pressure of 1×10^3 J Kg^{-1} K^{-1}. Such a small change in the potential temperature would make very little impact on the solution. More serious is the assumed absence of mixing of M and θ between the environment and the dome and within the dome itself as the air passes over the ridge.

How detrimental these assumptions are in practice can only be gauged through observational comparison. In the discussion to follow it is argued that these 'weir solutions' have many realistic properties: more so, in fact, than the standard sub-critical solutions obtained using the geostrophic momentum coordinate transformation.

4. Discussion

The main purpose of this paper so far has been to illustrate the utility of a geometric method for solving the semi-geostrophic equations describing the flow of a two-dimensional density current over two-dimensional orography. Solutions can be obtained for mountain ridges of super-critical height (in the sense defined by Eliassen (1980)) for which semi-geostrophic theory is often thought to be inapplicable - primarily because of the failure of the geostrophic momentum coordinate transformation to give single valued solutions. The Lagrangian solutions described here involve instantaneous 'jumps' between points in physical space and can only make physical sense if the propagation speed of the implied downslope current can be much greater than the uniform cross-ridge geostrophic flow. The mass transport rate in this implied weir is entirely controlled by the balanced dynamics embodied in the semi-geostrophic equations. The details of the weir itself of course cannot be described by these equations and even if the primitive equations were used, the resolution required to resolve the energy dissipation process would have to be very high indeed. Clearly if the semi-geostrophic solutions are to be of any value they must compare favourably with the observed behaviour of dammed cold air flows.

The existence of intense low-level jetstreams running parallel to mountain ridges has been reported by Schwerdtfeger (1975) and Parish (1982), both being related to the damming of cold air. Parish found winds of 15-30 ms^{-1} along the Sierra Nevada Mountains at levels below 2.7 km, particularly in association with the approach of cold fronts (Fig 9). These barrier jets were typically of 100 km horizontal extent and compare well with the semi-geostrophic solutions described here. Unfortunately, lee-side observations were not available to confirm the existence of a weir though primitive equation model results also in the paper showed strong downslope winds.

Conversely, Reed (1981) and Mass and Allbright (1985) describe lee-side windstorms in association with cold air dammed against the eastern side of the Cascade Mountains (Washington State, USA) though do not mention barrier jetstreams explicitly. Nevertheless, the potential temperature cross-sections they present are highly reminiscent of the cold air distribution found in the semi-geostrophic model. Cold air extends up the windward side of the Cascade Mountains forming a very stable layer near the mountain ridge crest. Potentially warm air exists on the lee-side above a 'bora-like' downslope current of great intensity. There is a hint of a cold air dome 100 Km downstream of the ridge in Reed's study though it is insufficiently resolved to justify comparison with the model. Large pressure differences across the mountain ridge were noted in both cases with peak values of about 17 mb. In the semi-geostrophic model, pressure differences are much smaller (~ 2-3 mb). This is in part due to the smallness of the assumed potential temperature difference between the

environment and the cold air dome (5°K compared to a cross-ridge difference of - 10°K in Reed's study). A further contribution can come from the 'lift' force (see Smith (1979)) associated with geostrophic flow parallel to the ridge but without cold air damming. For instance, in the bell-shaped mountain model of section 2 (c) a uniform geostrophic wind v_g could have been added to the solution without affecting the sequences of equilibrium states calculated. An additional pressure force proportional to the volume (area in this case) of the ridge would then act in the x direction. In practice, it would be difficult to distinguish lift from drag force though this difference is immaterial as far as their role in the momentum budget is concerned. Many other observational studies have found large pressure forces to act on mountain ridges (eg Davies and Phillips, 1985 and Smith, 1978). Hoinka (1985) noted a large discrepancy between the synoptic-scale pressure force acting on the Alps (1.6 - 7 Nm^2) in a south-Föehn event and the mid-tropospheric vertical momentum flux measured from an aircraft (0.3 Nm^{-2}) suggesting that much of the energy dissipation/wave radiation was taking place in the lower troposphere. The model described here strongly suggests that this synoptic-scale drag force was predominantly associated with cold air damming and local energy dissipation rather than vertically radiating gravity waves directly. Even so the gravity wave component in this situation still represents a powerful force on the atmosphere and would require parametrization. Although in the model air escapes <u>over</u> the mountain, in reality the release of dammed cold air may also take place around mountain ridges with similar effect.

The importance of these large drag forces in the atmospheric momentum budget cannot be over-emphasised (Palmer et al, 1985). Without some kind of representation of the mesoscale momentum sink they constitute, numerical models appear to exhibit a pronounced westerly wind bias in middle latitudes. In this respect the semi-geostrophic equations have, in principle, the ability to represent this physically important barrier effect without parametrization and implicitly account for the energy dissipation of unbalanced motion close to mountains. These 'weiring' solutions only occur when the radius of curvature of the mountain surface in $(x, \frac{Nz}{f})$ space is typically less than the Rossby radius of deformation based on the height of the mountain. Analytic models of uniform potential vorticity flow over sub-critical mountain ridges which have no drag force are therefore to be regarded as a rather restrictive class of solutions.

An interesting finding arising from the ALPEX project is the existence of very intense wind shears at the level of the mountain tops and upstream of the Alps during orographic blocking episodes. A pronounced (~ 90°) veering of the wind is often observed to occur in a layer little more than a 100 m deep and is accompanied by a marked inversion, (Pierrehumbert and Wyman, 1985). These phenomena have their direct counterparts in the model since the wind speed, direction and the potential temperature are all discontinuous at the dome interface. The directional shear is particularly noticeable close to the ridge where the barrier jet (almost parallel to the ridge) gives way to the uniform geostrophic basic state current in the warm air above. Of course, the agreement is to some extent 'built into' the model formulation by assuming two isentropic fluids. Even so it is possible to imagine the upwelling of dammed cold air in a continuously

stratified fluid leading to a layer of high static stability near and upstream of the point at which 'weiring' begins on the ridge. Such questions could be addressed by integrating a fully stratified, two-dimensional element model of the type described by Cullen et al (1986) though of considerably higher resolution.

Another obvious simplification of the model is that of two-dimensionality. Air parcels may be held up in their ascent of the windward side of the ridge for sufficient time to travel the length of a real mountain range and therefore go around rather than over the ridge. Rapid ageostrophic accelerations may then take place at the edge of the ridge as air becomes free to respond to the excess Coriolis force. Although three-dimensional element model solutions of the semi-geostrophic equations are possible in principle they would be very difficult to obtain in practice due mainly to the formidable computer logic required.

In summary, it has been found that the simple two-fluid semi-geostrophic model described here is capable of describing a class of physically interesting solutions which are outside the domain of validity of the geostrophic momentum coordinate transformation. These are relevant to the damming of cold air and the existence of large cross-mountain pressure differences. Solution of the semi-geostrophic equations proceeds by constructing a sequence of equilibrium states consistent with the Lagrangian conservation laws using a piece-wise constant representation of the absolute momentum and potential temperature fields. The model described here could be extended to three isentropic fluids using an iterative approach to determine the two interface configurations. In

general it would probably be better to extend the element model of Cullen et al (1986) to cases with smooth orographic profiles and larger numbers of elements. Only then would the comparison of the modelled cold air damming mechanism and Föehn effect with observations be fully justified.

References

Bannon, P. R. 1985 'Flow acceleration and mountain drag'. J.Atmos. Sci., 42, 2445-2453.

Blumen, W. and Gross, B. D. 1986 'Semi-geostrophic disturbances in a stratified shear flow over a finite-amplitude ridge'. Submitted to J.Atmos. Sci.

Cullen, M. J. P. 1983 'Solutions to a model of a front forced by deformation'. Quart.J. Roy. Met. Soc., 109, 565-573.

Cullen, M. J. P.and Parrett, C. A. 1986 'Mountain wave generation by models of flow over synoptic scale orography'. (Revised for Quart. J. Roy. Met. Soc.)

Cullen, M. J. P., Chynoweth, S. and Purser, R. J. 1986 'On semi-geostrophic flow over synoptic scale topography'. (Revised for Quart. J. Roy. Met. Soc.)

Davies, H. C. 1984 'On the orographic retardation of a cold front'. Contrib. to Atmos. Phys., 57, 409-418.

Davies, H. C. and Phillips, P. D. 1985 'Mountain drag along the Gotthard Section during ALPEX'. J. Atmos. Sci., 42, 2093-2109.

Eliassen, A. 1980 'Balanced motion of a stratified, rotating fluid induced by bottom topography'. Tellus, 32, 537-547.

Gill, A. E. 1981 'Homogeneous intrusions in a rotating stratified fluid'. J. Fluid Mech., 103, 275-295.

Hoskins, B. J. 1975 'The geostrophic momentum approximation and the semi-geostrophic equations'. J. Atmos. Sci., 32, 233-242.

Hoskins, B. J. and Bretherton, F. P. 1972 'Atmospheric frontogenesis models: mathematical formulation and solution'. J. Atmos. Sci., 29, 11-37.

Lamb, H. 1932 'Hydrodynamics' Cambridge Uni. Press, London.

Mass, C. F. and Albright, M. D. 1985 'A severe windstorm in the lee of the Cascade Mountains of Washington State'. Mon. Wea. Rev., 113, 1261-1281.

Merkine, L. O. 1975 'Steady finite-amplitude baroclinic flow over long topography in a rotating, stratified atmosphere'. J. Atmos. Sci., 32, 1881-1893.

Palmer, T. N., Shutts, G. J. and Swinbank, R. 1986 'Alleviation of a systematic westerly bias in general circulation and numerical weather prediction models through an orographic gravity wave drag parametrization'. (To appear Quart. J. Roy. Met. Soc., October)

Parish, T. 1982 'Barrier winds along the Sierra Nevada Mountains'. J. Appl. Met., 21, 925-930.

Pierrehumbert, R. T. 1985 'Stratified semi-geostrophic flow over two-dimensional topography in an unbounded atmosphere'. J. Atmos. Sci., 42, 523-526.

Pierrehumbert, R. T and Wyman, B. 1985 'Upstream effects of mesoscale mountains'. J. Atmos. Sci., 42, 977-1003.

Powell, M. J. D. 1970 'A hybrid method for non-linear algebraic equations'. From 'Numerical methods for Non-linear Algebraic Equations', Ed. Rabinowitz, P., Gordon and Breach.

Purser, R. J. and Cullen, M. J. P. 1986 A semi-geostrophic duality principle'. (in preparation).

Reed, R. J. 1981 'A case study of a bora-like windstorm in western Washington'. Mon. Wea. Rev., 109, 2383-2393.

Schwerdtfeger, W. 1975 The effect of the Antarctic Peninsula on the temperature regime of the Weddell Sea'. Mon. Wea. Rev., 103, 45-51.

Smith, R. B. 1978 'A measurement of mountain drag'. J. Atmos. Sci., 35, 1644-1654.

Smith, R. B. 1979 'The influence of mountains on the atmosphere'. Adv. in Geophys., 21, 87-230.

Wallace, J. M., Tibaldi, S. and Simmons, A. J. 1983 'Reduction of systematic errors in the ECMWF model through the introduction of an envelope orography'. Quart. J. Roy. Met. Soc., 109, 683-718.

Legends

Fig. 1 Uniform flow over a two-dimensional ridge with elliptical cross-section.

(a) Potential temperature field. Contour interval, 2°K.

(b) Along-ridge geostrophic wind, v_g. Contour interval, 0.5 ms^{-1}.

Fig. 2 Uniform flow over a two-dimensional ridge of semi-circular cross-section.

(a) Potential temperature field. Contour interval, 0.5°K.

(b) Along-ridge geostrophic wind, v_g. Contour interval, 1 ms^{-1}.

Fig. 3 Element model representation of a cold air dome on a horizontal plane.

Figs. 4 (a)-(e) A sequence of model states for flow over a rectangular block mountain corresponding to times 0, 250, 500, 900, 1300 minutes respectively.

Figs. 5 (a)-(f) A sequence of model states for flow over a bell-shaped mountain at intervals of 4×10^4s. Element boundaries are not indicated. Graphs of v_g corresponding to the fluid below are inset.

Figs. 6 (a)-(c) Two-dimensional tank of liquid containing a rectangualr obstacle. (a)-(c) give three equilibrium states when the block is moved to the left. The system is non-rotating.

Fig. 7 The drag force on the bell-shaped mountain during the passage of a cold air dome.

Fig. 8 Plots of the work done by the drag force ($\overline{E}$) and the model's semi- geostrophic energy ($\overline{E}_g$) corresponding to Fig. 7.

Fig. 9 Observed barrier jet along the Sierra Nevada range from Parrish (1982).

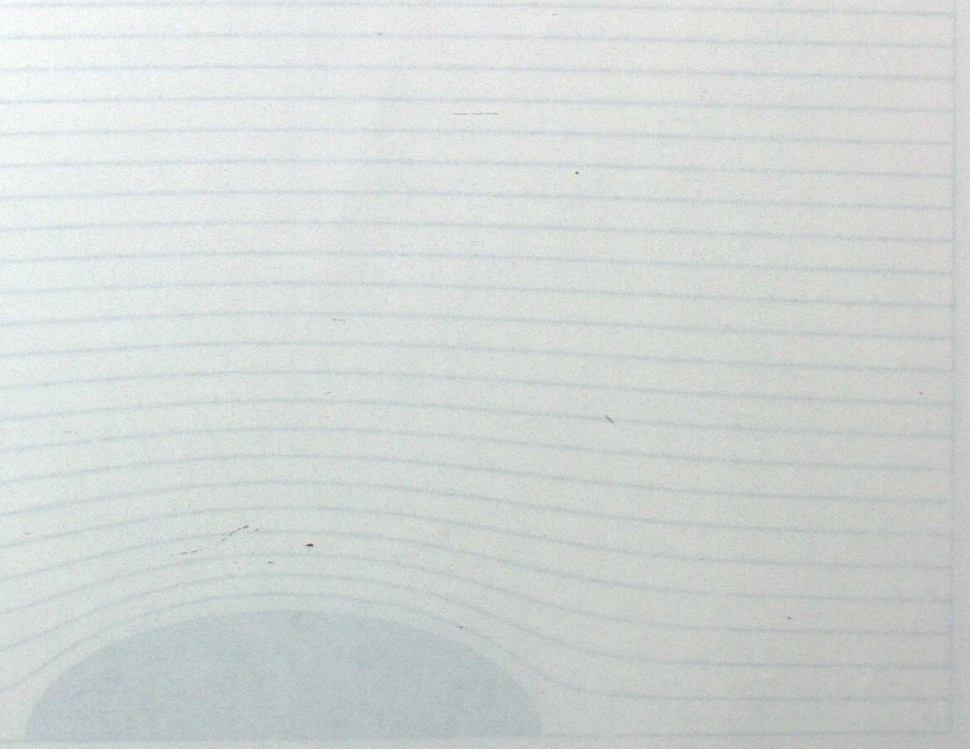

Fig. 1 (a)

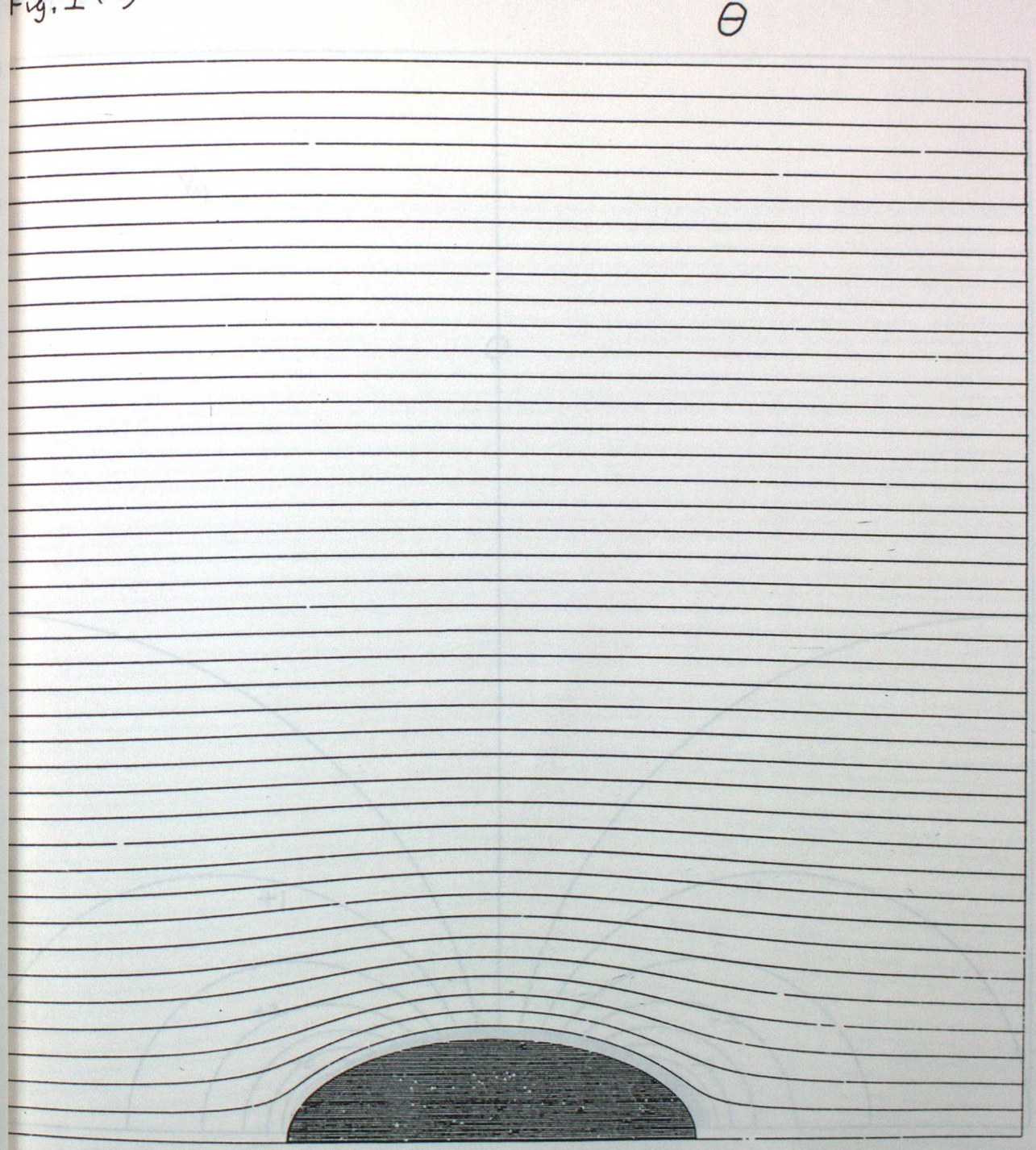

Fig. 1 (b)

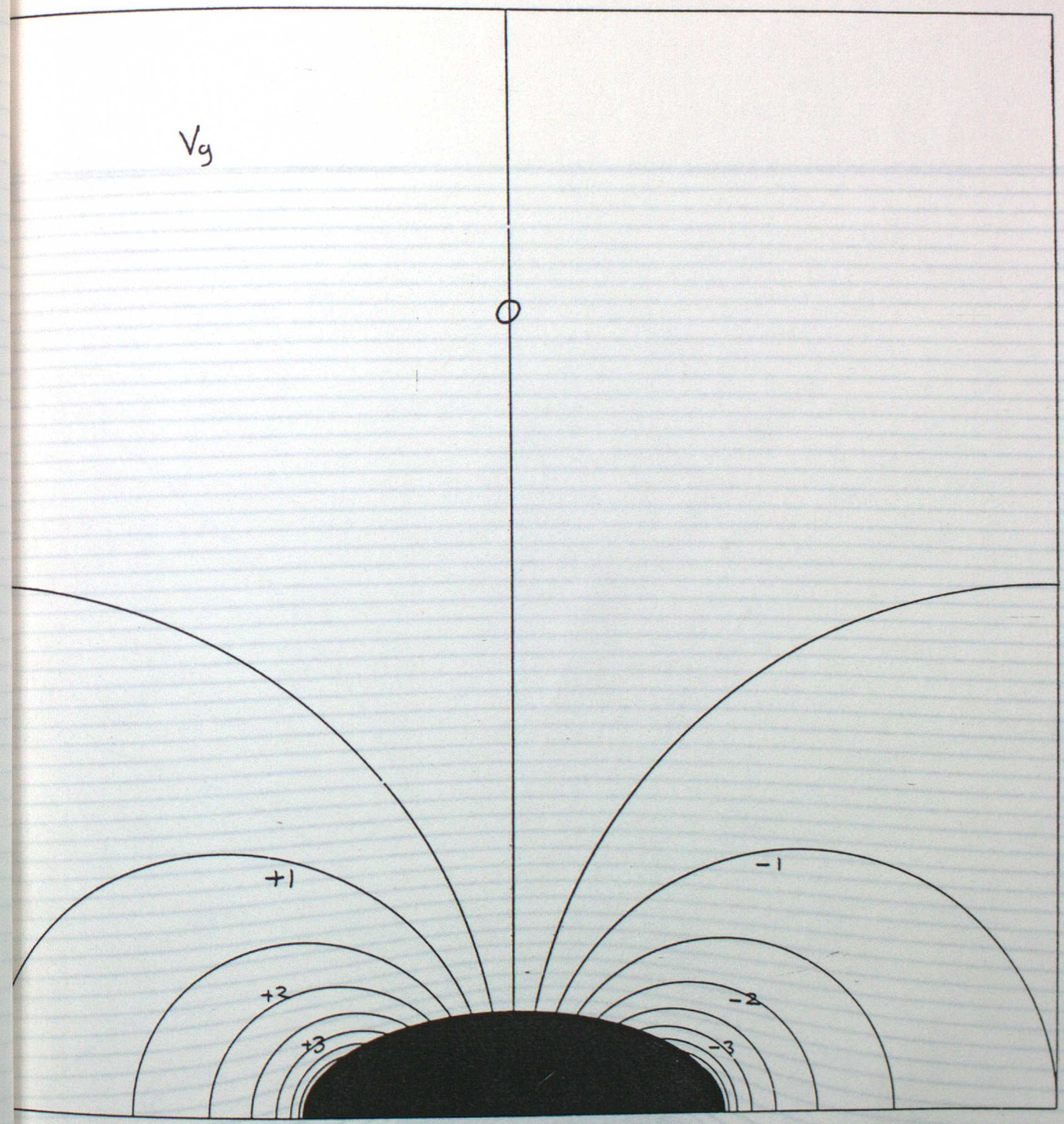

Fig. 2(a)

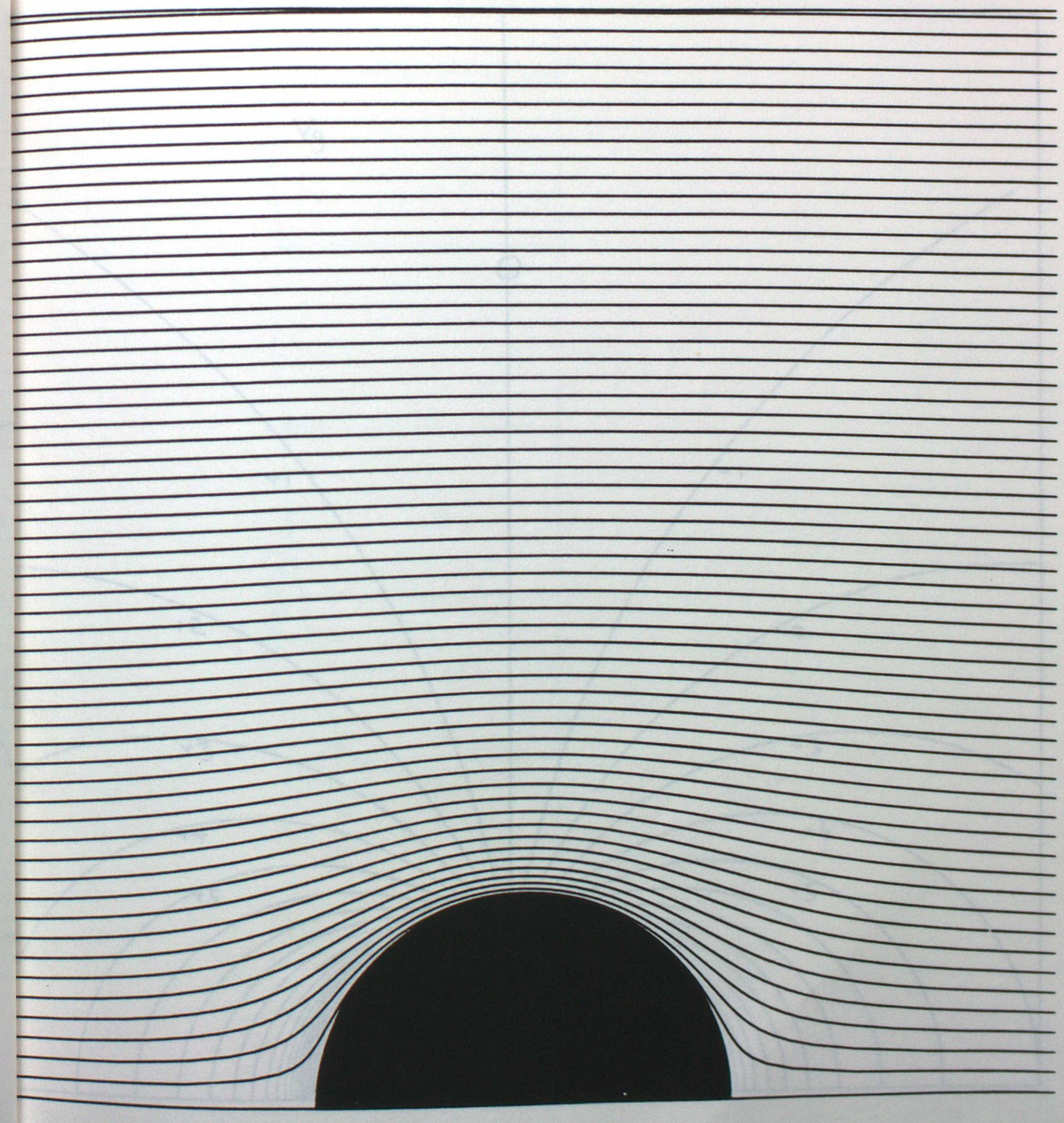

g. 2(b)

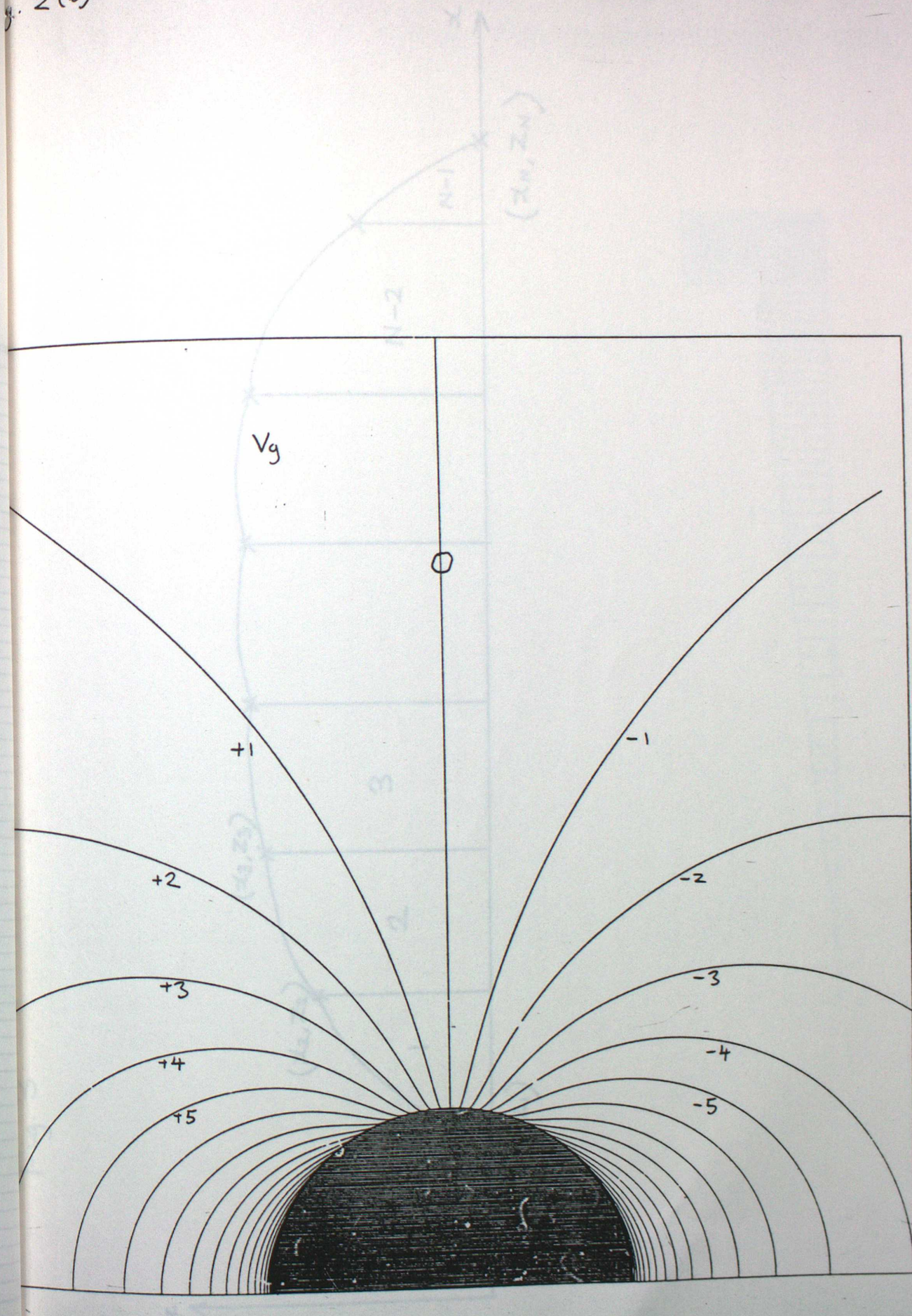

Fig. 3

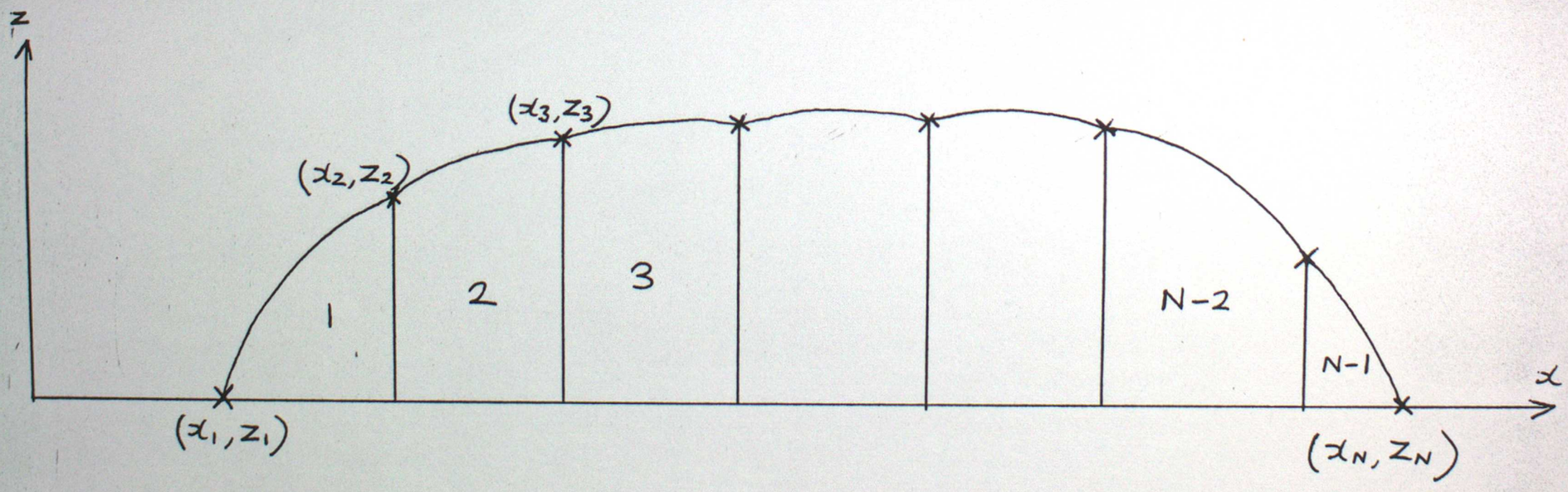

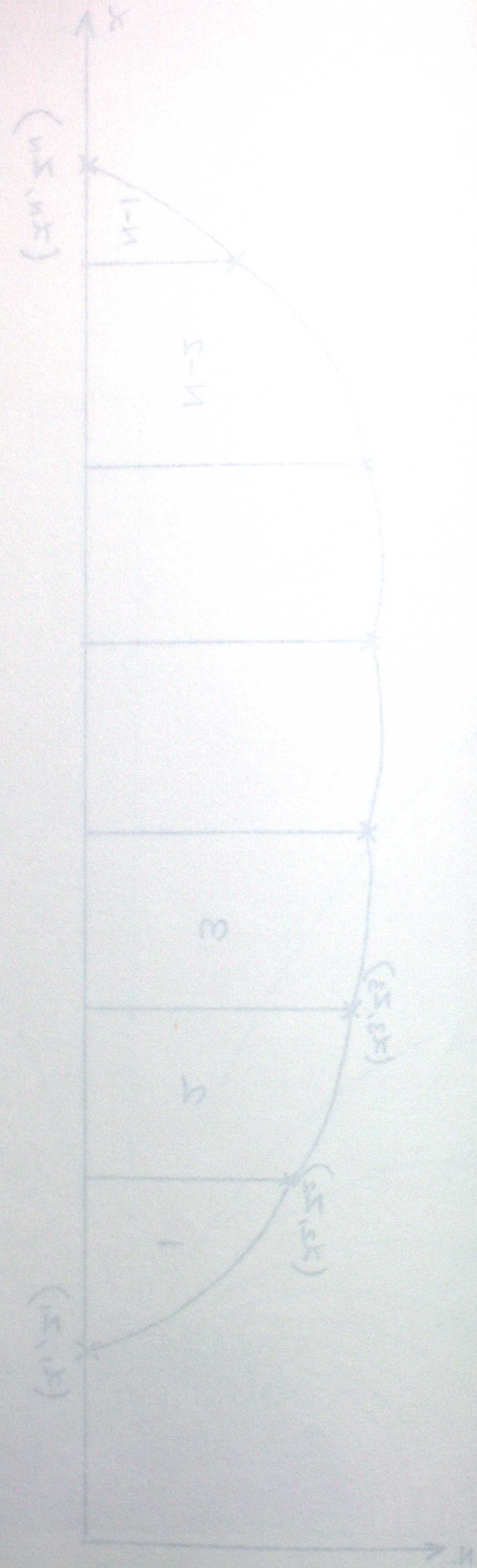
x
k
n-s
d
c
b
a
u

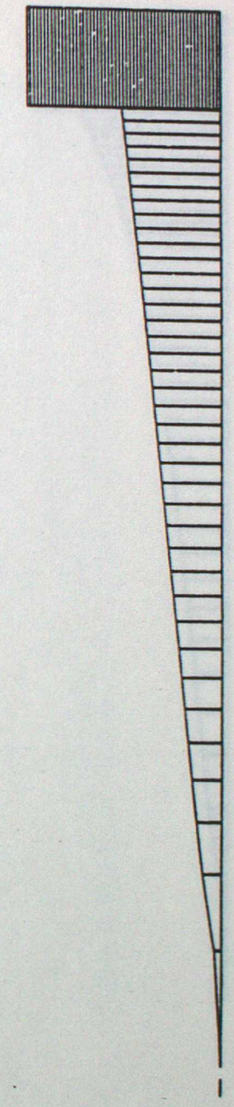

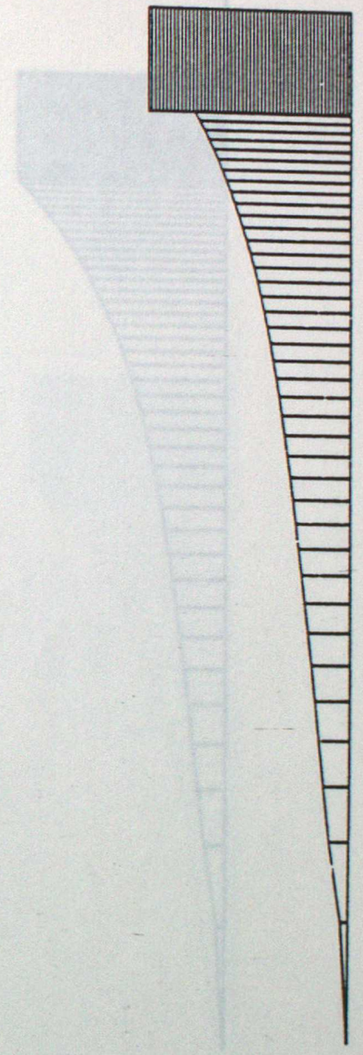

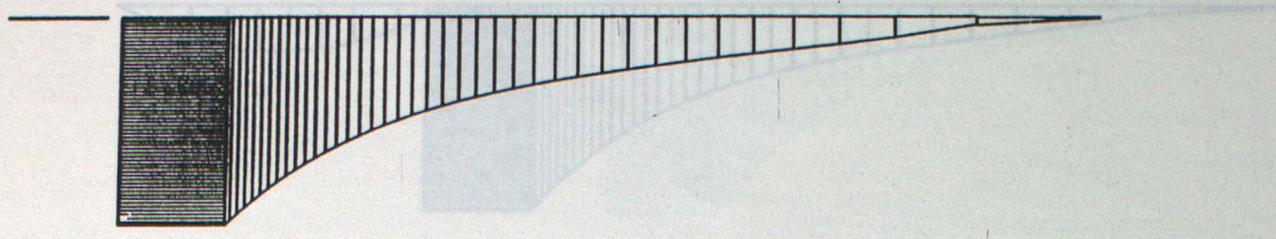

Fig. 4 (c)

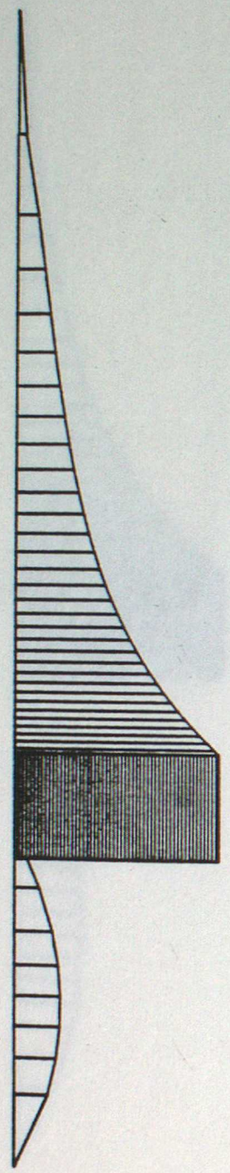

Fig. 4 (a)

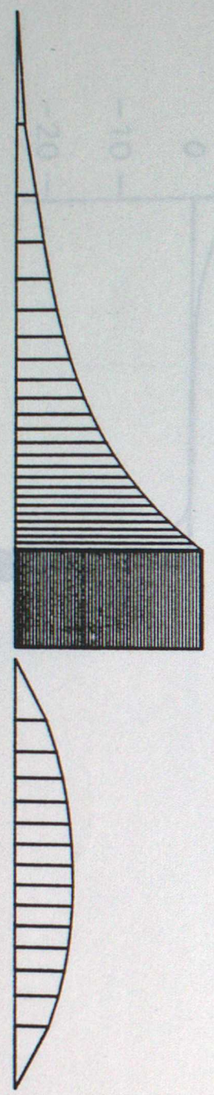

Fig. 4(e)

Fig. 5 (a)

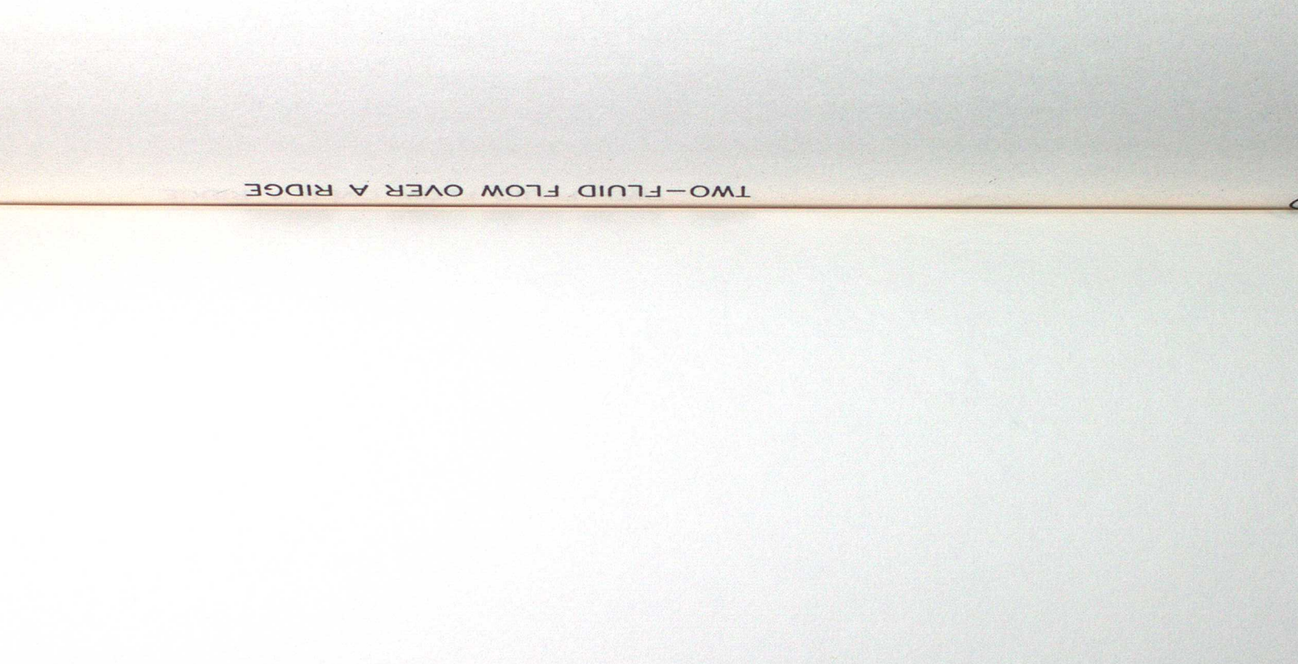

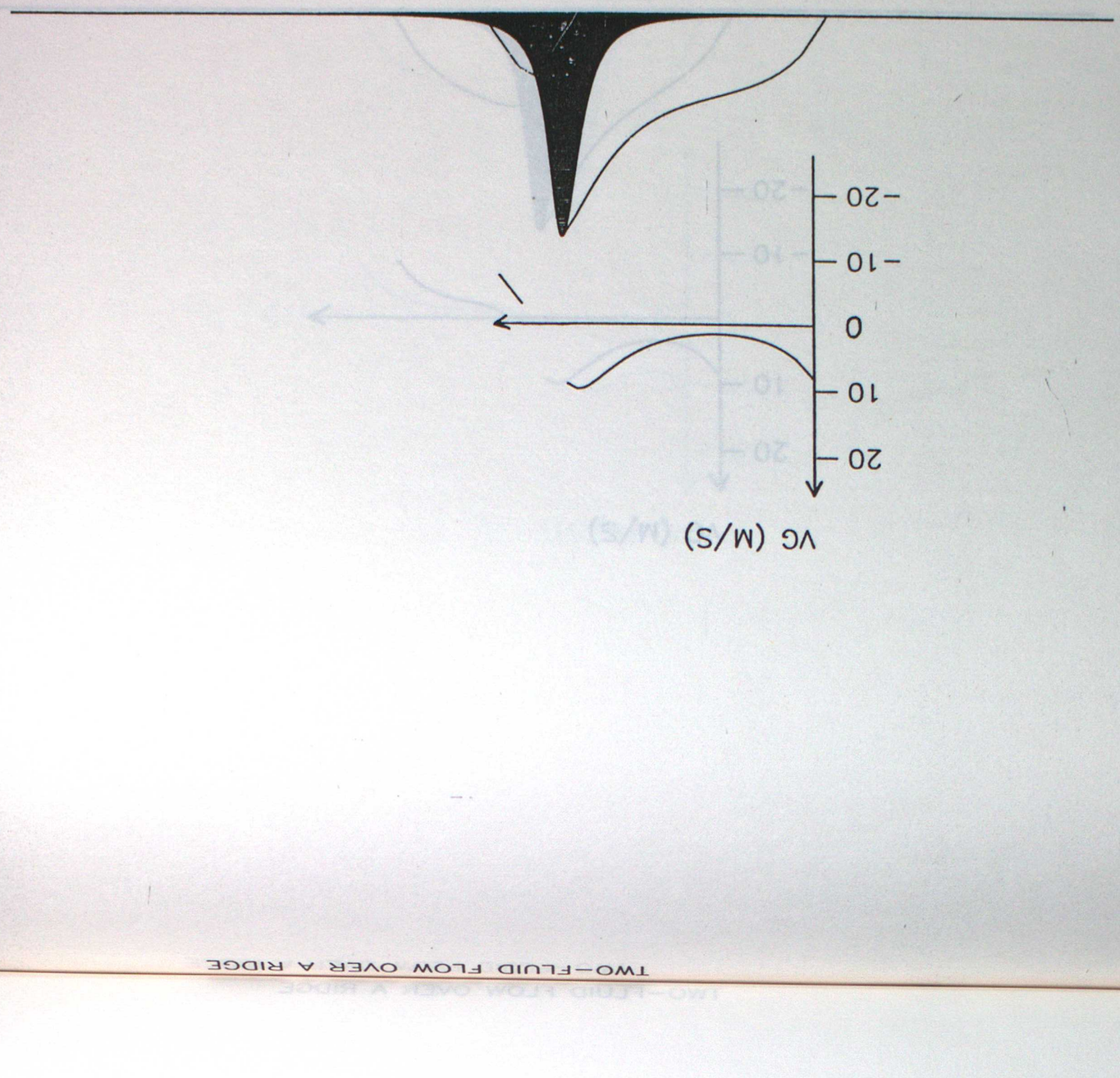
VG (M/S)
20
10
0
-10
-20

Fig. 5.6(c)

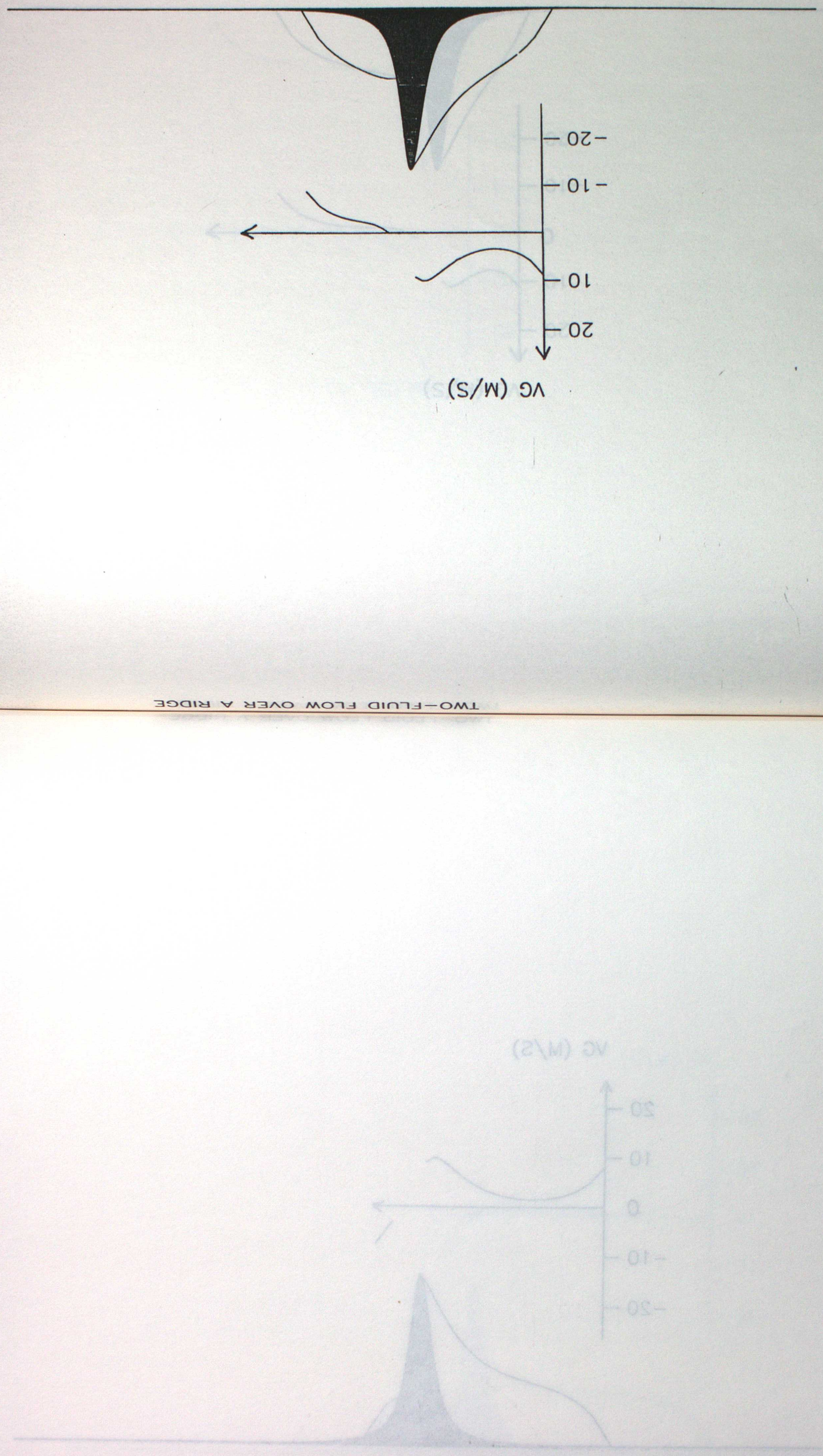

Fig. 5(a)

TWO-FLUID FLOW OVER A RIDGE

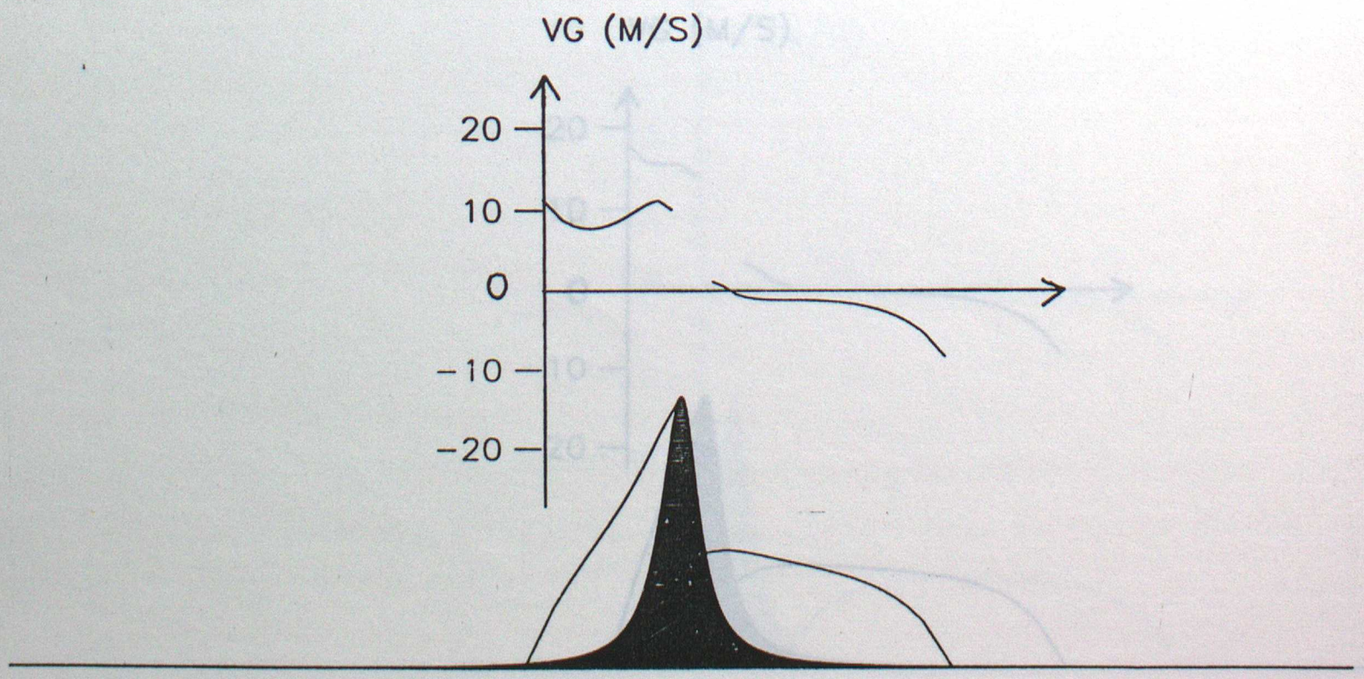

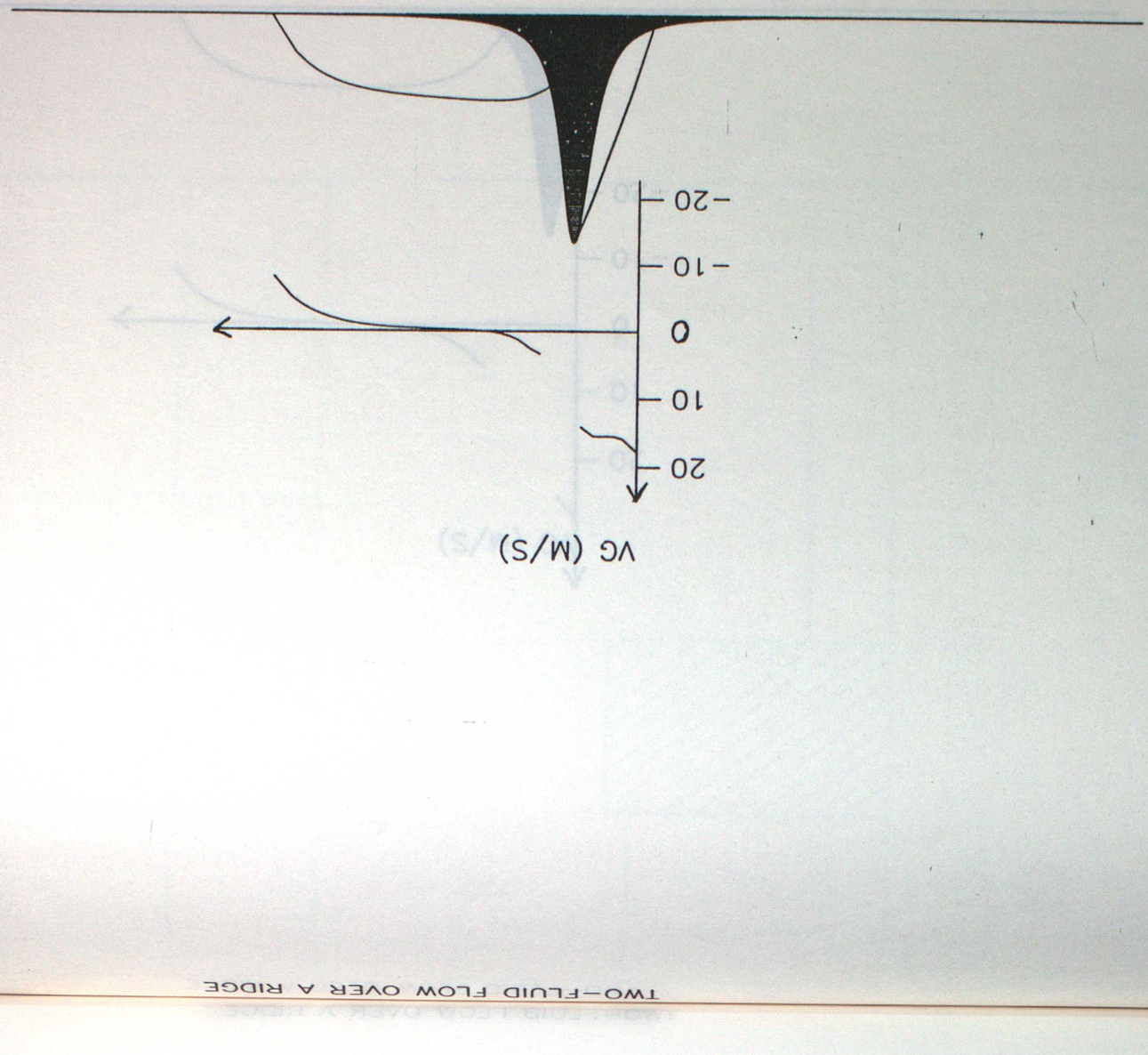

Fig. 5 (c)

TWO-FLUID FLOW OVER A RIDGE

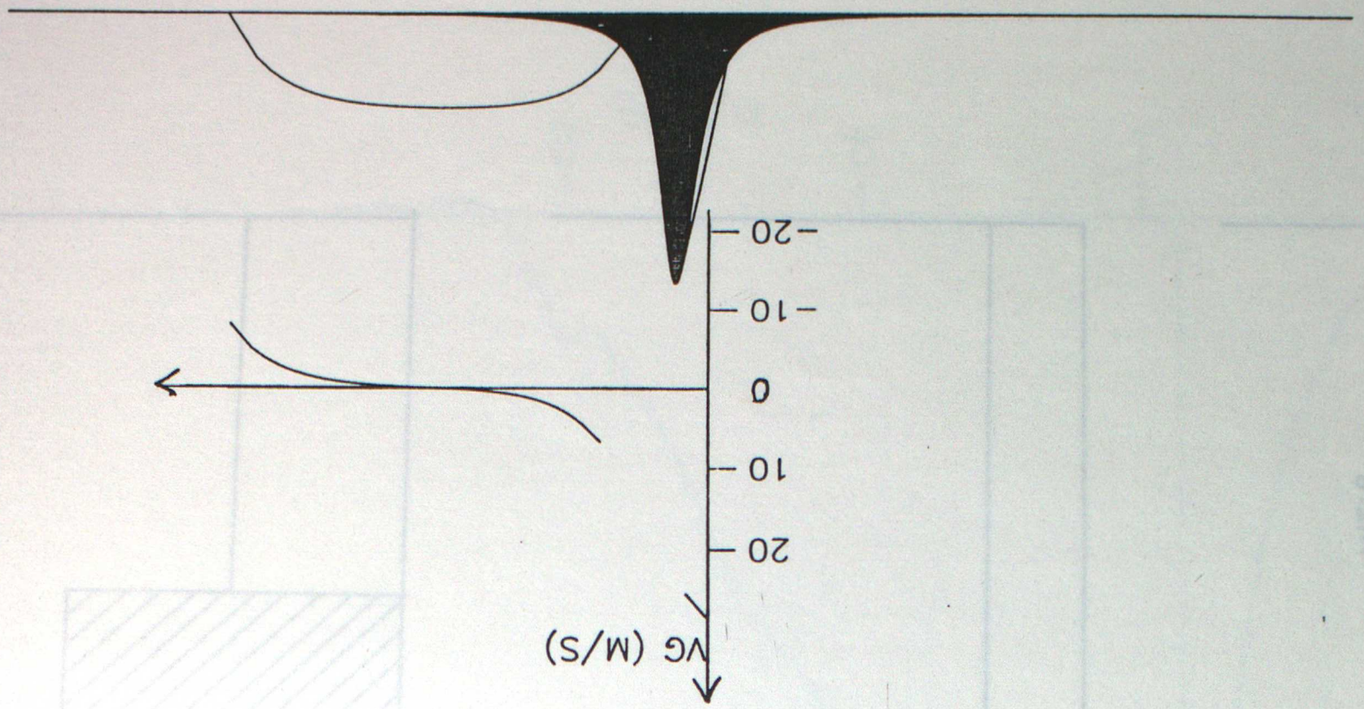

TWO-FLUID FLOW OVER A RIDGE

Fig. 5.47

Fig. 6

(a)

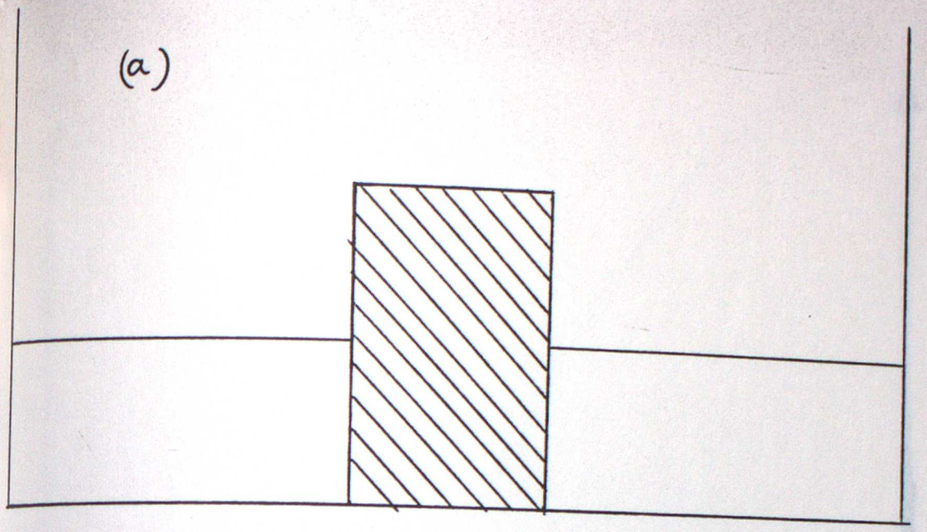

(b)

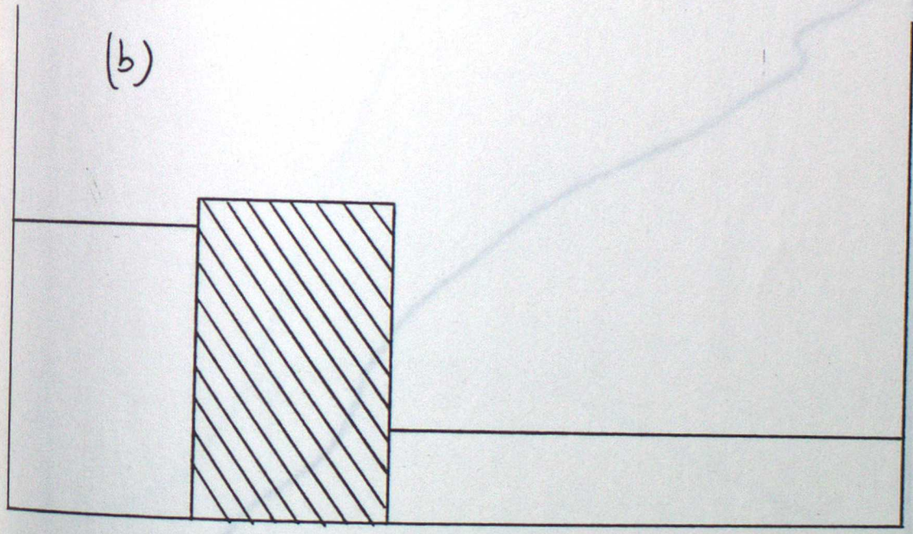

(c)

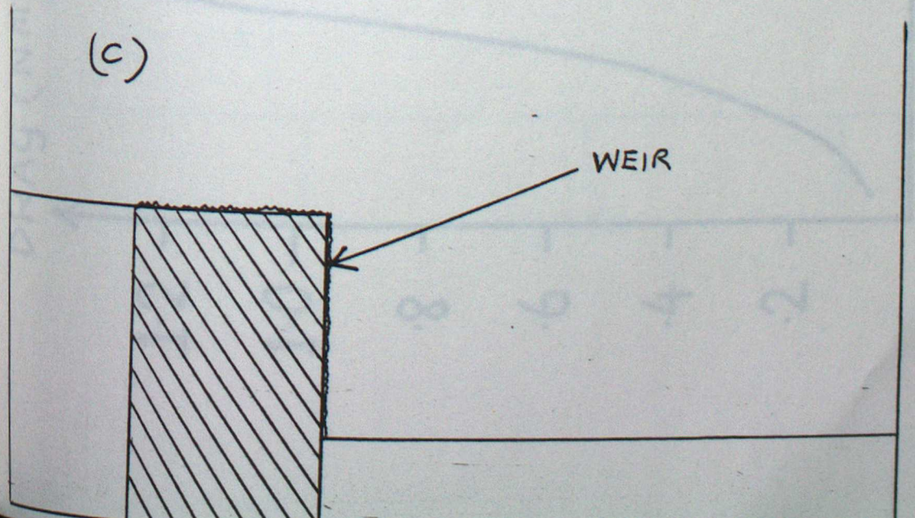

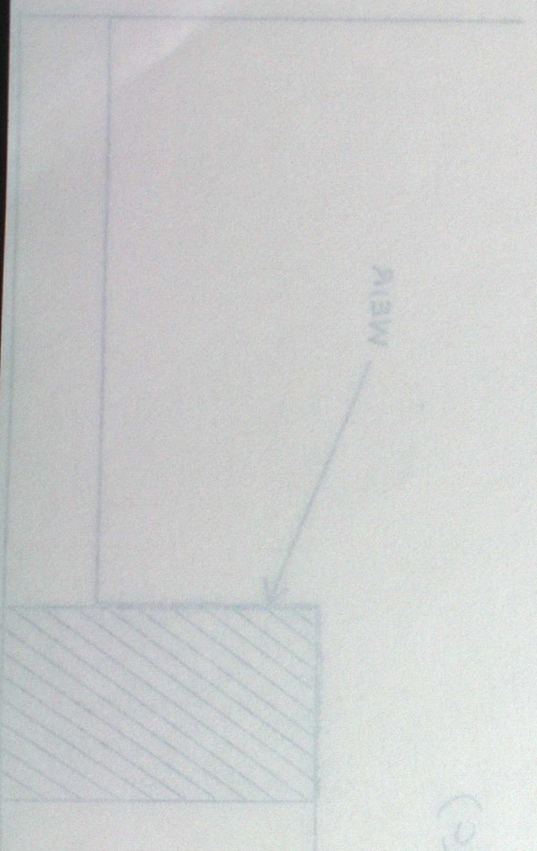
MEAN

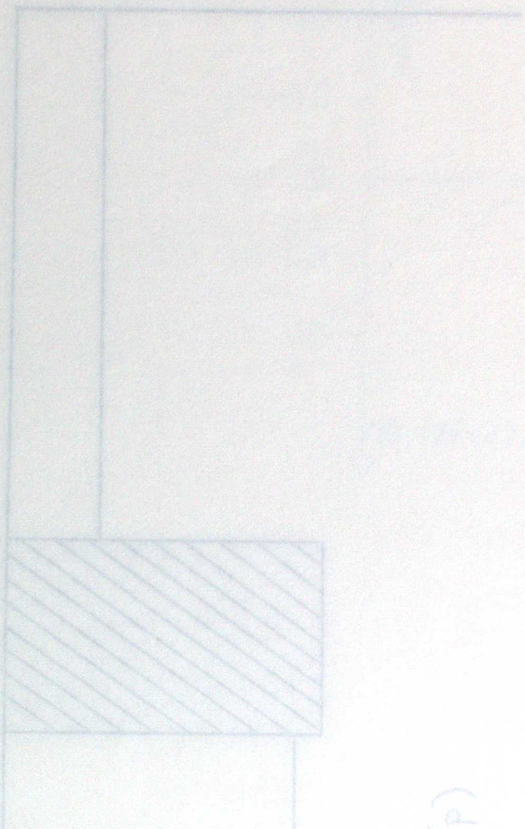

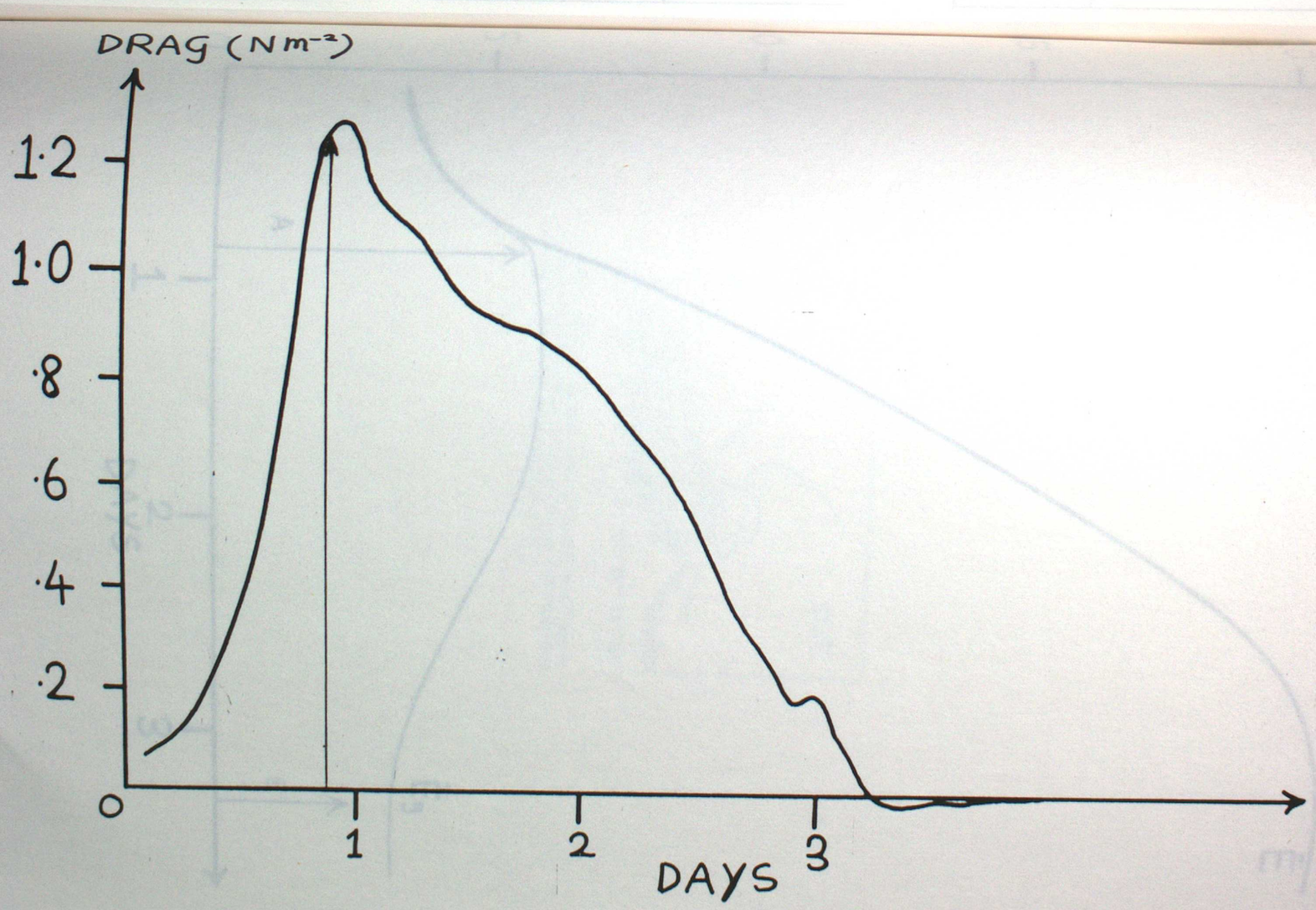
DRAG (N m⁻²)
1·2
1·0
·8
·6
·4
·2
0
1
2
3
DAYS

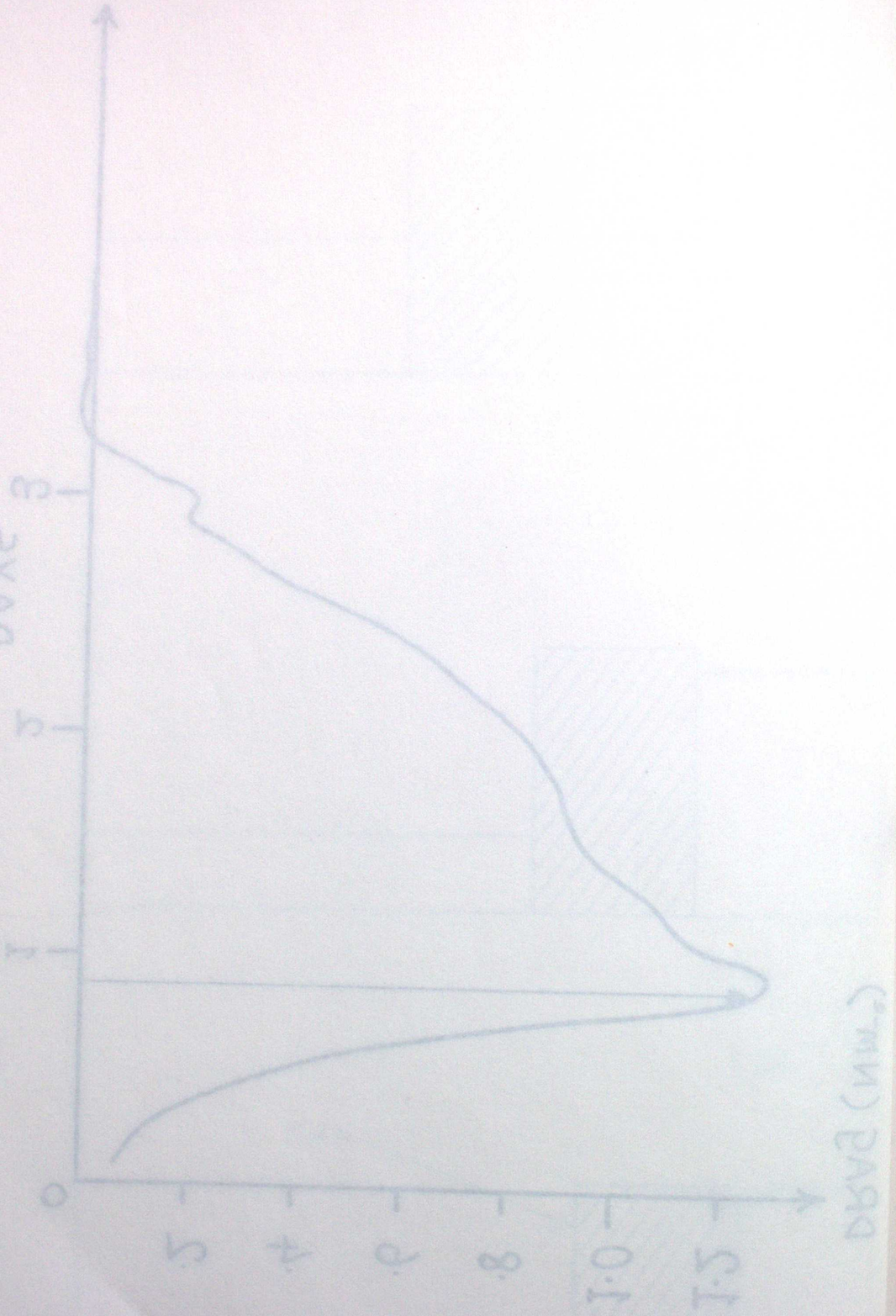
DAYS (MWe)
0
1
2
3
4
5
6
7
8
9
10
11

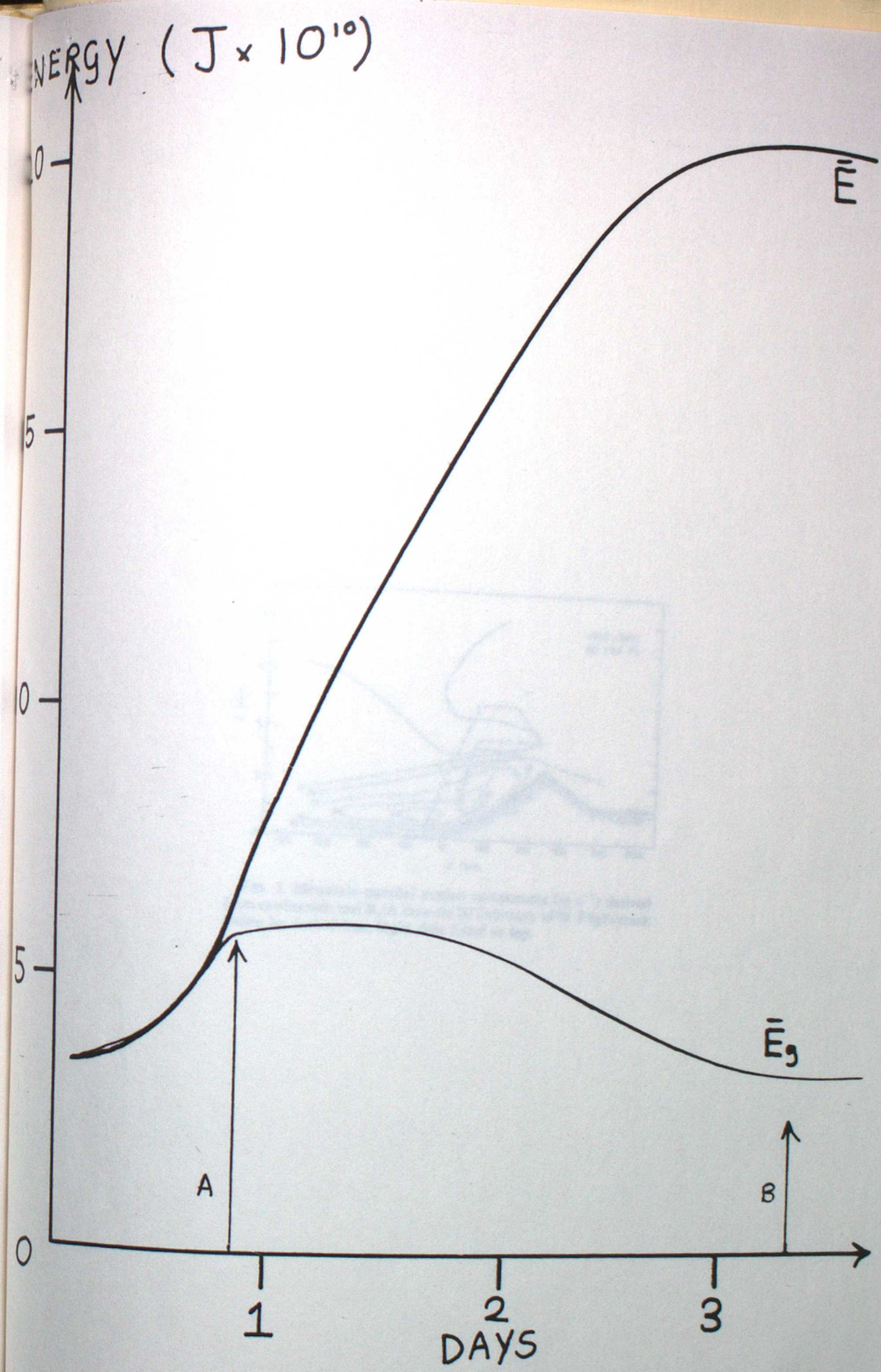
ENERGY (J × 10¹⁰)
10
5
0
Ē
Ē₉
A
B
1
2
3
DAYS

Fig. 9.

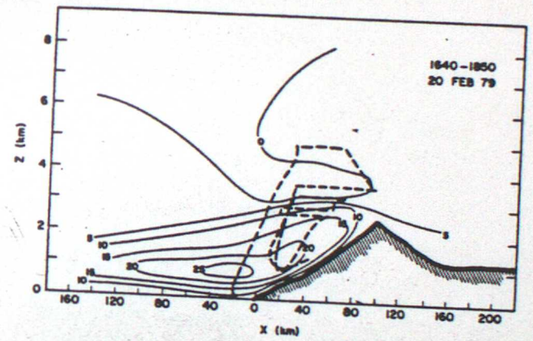

FIG. 5. Mountain-parallel motion components (m s^{-1}) derived from rawinsonde and K/A data for 20 February 1979. Flight track shown by dashed line; flight time listed at top.